AD-A163 409 WAVES AND ELECTRIC FIELDS ASSOCIATED WITH THE DECEMBER 27 1984 ARTIFICIAL..(U) IOWA UNIV IOWA CITY DEPT OF PHYSICS AND ASTRONOMY D A GURNETT ET AL. 27 NOV 85 1/1

UNCLASSIFIED U. OF IOWA-85-18 N00014-82-K-0183 F/G 4/1 NL

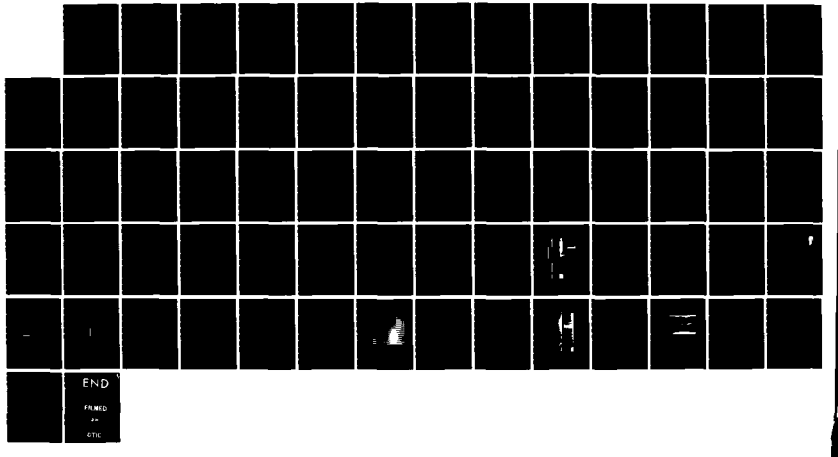

END

FILMED

+-

DTIC

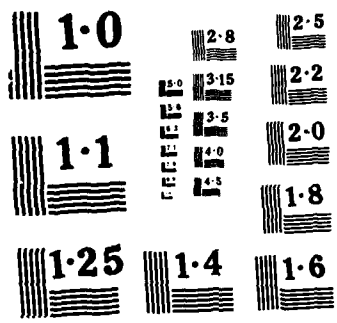

WAVES AND ELECTRIC FIELDS ASSOCIATED WITH THE DECEMBER 27, 1984, ARTIFICIAL COMET

by

D. A. Gurnett[1], T. Z. Ma[1], R. R. Anderson[1],
G. Haerendel[2], G. Paschmann[2], O. H. Bauer[2],
R. A. Treumann[2], H. C. Koons[3],

Department of Physics and Astronomy
THE UNIVERSITY OF IOWA
Iowa City, Iowa 52242

UNCLASSIFIED

SECURITY CLASSIFICATION OF THIS PAGE (When Data Entered)

REPORT DOCUMENTATION PAGE		READ INSTRUCTIONS BEFORE COMPLETING FORM
1. REPORT NUMBER U. of Iowa 85-18	2. GOVT ACCESSION NO. AD-A163 409	3. RECIPIENT'S CATALOG NUMBER
4. TITLE (and Subtitle) Waves and Electric Fields Associated With the December 27, 1984, Artificial Comet		5. TYPE OF REPORT & PERIOD COVERED Progress November 1985 6. PERFORMING ORG. REPORT NUMBER
7. AUTHOR(s) D. A. Gurnett, T. Z. Ma, R. R. Anderson, G. Haerendel, G. Paschmann, O. H. Bauer, R. A. Treumann, H. C. Koons, R. Holzworth and H. Luhr		8. CONTRACT OR GRANT NUMBER(s) N00014-82-K-0183 N00014-85-K-0404
9. PERFORMING ORGANIZATION NAME AND ADDRESS Department of Physics and Astronomy The University of Iowa Iowa City, IA 52242		10. PROGRAM ELEMENT, PROJECT, TASK AREA & WORK UNIT NUMBERS
11. CONTROLLING OFFICE NAME AND ADDRESS Electronics Program Office Office of Naval Research Arlington, VA 22217		12. REPORT DATE 27 November 1985 13. NUMBER OF PAGES 67
14. MONITORING AGENCY NAME & ADDRESS(if different from Controlling Office)		15. SECURITY CLASS. (of this report) Unclassified 15a. DECLASSIFICATION/DOWNGRADING SCHEDULE

16. DISTRIBUTION STATEMENT (of this Report)

Approved for public release; distribution is unlimited.

17. DISTRIBUTION STATEMENT (of the abstract entered in Block 20, if different from Report)

18. SUPPLEMENTARY NOTES

19. KEY WORDS (Continue on reverse side if necessary and identify by block number)

AMPTE
Electric Fields
Artificial Comet
Solar Wind

20 ABSTRACT (Continue on reverse side if necessary and identify by block number)

(See following page)

DD FORM 1 JAN 73 1473 EDITION OF 1 NOV 65 IS OBSOLETE
S/N 0102-LF-014-6601

Unclassified
SECURITY CLASSIFICATION OF THIS PAGE (When Data Entered)

ABSTRACT

A variety of plasma wave and electric field effects were observed during the AMPTE (Active Magnetospheric Particle Tracer Explorers) solar wind barium release ~~on December 27, 1984~~. Electron plasma oscillations at the local electron plasma frequency provided measurements of the electron density during the entire event. Inside the diamagnetic cavity created by the ion cloud, the electron density reached a peak of about 2×10^5 cm^{-3}, then decreased approximately as t^{-2} as the cloud expanded. A static electric field of about 1 to 2 mVolt/m was detected in the diamagnetic cavity. This electric field is in the same direction as the solar wind electric field, suggesting that polarization charges in the ion cloud are not effective at shielding out an external electric field. As the spacecraft passed through the boundary of the diamagnetic cavity, a region of compressed plasma and magnetic field was detected upstream of the ion cloud with a peak density of about 10^4 cm^{-3} and magnetic field strength of 130 nT. This region of compressed plasma is believed to be caused by solar wind plasma and magnetic field lines draped around the noise of the ion cloud.

Inside the diamagnetic cavity electrostatic emissions were observed in a narrow band centered on the barium ion plasma frequency and in another band at lower frequencies. These waves are believed to be short wavelength ion acoustic waves. Bursts of electrostatic waves were also observed at the boundaries of the diamagnetic cavity,

apparently caused by an electron drift current along the boundary. Near the outer boundary of the plasma compression region, an intense burst of broadband electrostatic noise was observed with intensities of up to 140 mVolts/m. This noise is apparently associated with a shock-like interaction between the ion cloud and the solar wind. Growth rate computations show that this noise can be accounted for by an electrostatic ion beam-plasma interaction between the nearly stationary barium ions and the rapidly moving solar wind protons.

I. INTRODUCTION

The first attempt to produce a man-made comet was performed on December 27, 1984, as part of the AMPTE (Active Magnetospheric Particle Tracer Explorers) program. The primary objective of the AMPTE program was to use artificially injected barium and lithium ions as tracers to study the transport and energization of charged particles in the earth's magnetosphere [Krimigis et al., 1982]. A secondary objective was to simulate the solar wind-plasma interactions of a natural comet by releasing a cloud of barium gas in the solar wind. The possibility of simulating a comet by artificial gas releases in the upper atmosphere was first suggested by Biermann et al. [1961]. Since the original suggestion by Biermann et al. numerous gas releases were performed in the ionosphere and lower magnetosphere using explosive canisters carried aloft by rockets [Haerendel et al., 1967; Haerendel and Lüst, 1968]. However, the first true artificial comet, intended to simulate the interaction with the solar wind, was carried out by the AMPTE project. Two artificial comet releases were performed: the first on December 27, 1984, and the second on July 18, 1985. The purpose of this paper is to provide a detailed discussion and analysis of the plasma wave observations obtained during the first release on December 27, 1984. The second release will be discussed in a future paper.

The AMPTE project consists of three spacecraft: the Ion Release Module (IRM) which carried the barium and lithium canisters, the United Kingdom Satellite (UKS) which flew near the IRM to study the expansion and evolution of the ion cloud, and the Charge Composition Explorer (CCE) which was intended to detect the tracer ions in the inner regions of the magnetosphere. The data presented in this paper are from the IRM. The IRM is in a low-inclination, highly eccentric orbit with an apogee geocentric radial distance of about 19 R_E. The barium cloud was produced by releasing two canisters containing barium in diametrically opposite directions from the IRM. Ten minutes after the release the two canisters were exploded simultaneously at a distance of about 1 km from the spacecraft. The explosions produced a rapidly expanding cloud of neutral barium which swept over the spacecraft a fraction of a second later. As the cloud expanded, ultraviolet radiation from the sun ionized the gas, forming a dense cloud of ionized barium. For barium the ionization time constant is quite short, only about 28 seconds, which is one of the reasons that this element is used. For a discussion of the physics of the cloud formation and expansion, see Haerendel [1983].

A wide variety of particle and field instruments were used on the IRM to analyze plasma effects produced by the ion cloud. A list of all the instruments on the spacecraft is given by Krimigis et al. [1982]. The measurements of particular interest for this paper are from the plasma wave instrument, the plasma instrument, and the magnetometer.

The plasma wave instrument uses a 47m tip-to-tip electric dipole antenna for electric field measurements and two search coil magnetometers for magnetic field measurements. The signals from these antennas are processed by a variety of receivers and analyzers provided by three groups: the University of Iowa, the Max-Planck-Institut, and the Aerospace Corporation. This combined instrumentation provides spectrum measurements from 0 to 6 MHz for the electric field, and from 30 Hz to 11041z for the magnetic field. For a description of the plasma wave instrument, see Häusler et al. [1985a]. The plasma instrument on the IRM provides full three-dimensional measurements of the electron and ion distribution functions once every spacecraft rotation (~ 4.4 sec). The energy range is 15 to 30 keV/q for electrons and 20 to 40 keV/q for ions. For a description of the plasma instrument, see Paschmann et al. [1985]. The magnetic field instrument on the IRM is a three-axis magnetometer with a dynamic range of 0.1 to 60,000 nT. For a description of the magnetometer, see Lühr et al. [1985a].

The first AMPTE artificial comet experiment was performed on December 27, 1984. The canisters were released at 1222:00 UT and exploded at 1232:00 UT. The distance between the canisters and the spacecraft at the time of the explosion is estimated to be 0.87 km. The IRM at this time was in the solar wind on the morning side of the earth at a geocentric radial distance of 17.2 R_E and a local time of 7.1 hours. The barium ion cloud produced by the explosion was observed on the ground for a period of several minutes. For an initial report

on the optical, plasma, magnetic field, and plasma wave effects observed during this release, see the series of papers by Haerendel et al. [1985], Valenzuela et al. [1985], Rees et al. [1985], Lühr et al. [1985], Rodgers et al. [1985] and Gurnett et al. [1985].

II. PLASMA DENSITY

One of the primary objectives of the plasma wave investigation on the IRM was to measure the density of the ion cloud produced by the explosion. Two effects provided a determination of the plasma density from the plasma wave data. The first effect is the presence of electrostatic oscillations at the electron plasma frequency. These oscillations can be seen in the spectrogram of Figure 1 starting shortly after the explosion at 1232:00 and extending to about 1234:20. The narrow-band character of the emissions and their similarity to previous spacecraft observations [Scarf et al., 1971] uniquely identifies these waves as electron plasma oscillations. Because the oscillations are at the local electron plasma frequency, which is given by $f_p = 9000 \sqrt{N_e}$ Hz, where N_e is the electron number density in cm^{-3}, a measurement of the emission frequency gives the local electron density. The second effect is the presence of a propagation cutoff in the galactic and terrestrial radio emissions. This cutoff can be clearly seen in Figure 1 about a factor of two above the local electron plasma frequency. The cutoff is caused by the high electron density in the cloud which blocks all external radiation at frequencies below the electron plasma frequency. As is well known [Krall and Trivelpiece, 1973], free space electromagnetic radiation cannot propagate at frequencies below the electron plasma frequency.

The top panel of Figure 2 shows the electron density variations obtained from the electron plasma oscillations. Each point represents a single sweep of the spectrum analyzer. As can be seen, within a fraction of a second after the explosion, the electron density jumps nearly five orders of magnitude, up to about 2×10^5 cm^{-3}, then decays back to the ambient solar wind density over a period of about 2 minutes. For a few brief periods, particularly early in the event, the plasma oscillations were too weak to provide reliable measurements. The density profile is interpolated through these regions by a straight line. After about 1234:25 the electron plasma oscillations become very difficult to identify. Other less well-resolved emissions at lower frequencies suggest that the electron density continues to decline steeply, as indicated by the dashed line. The solid horizontal line shows the nominal solar wind density before the event. Barium ions are believed to constitute the dominant component of the cloud from 1232:00 to at least 1234:25, after which the solar wind protons are dominant. Since the barium ions are singly charged and the plasma is electrically neutral, the barium ion density in the central region of the cloud is approximately equal to the electron density, $N_{Ba^+} = N_e$.

Interpretation

The density variations at the IRM are controlled by two processes, expansion and convection. During the expansion phase, which extends up to about 1233, the density decreases monotonically as the cloud expands radially outward. The expansion phase continues until about 1233:15,

with the density varying approximately as t^{-2}. During the expansion phase the spacecraft is in a region of essentially zero magnetic field created by the expanding ion cloud. For comparison the magnetic field is shown in the bottom panel of Figure 2. The region of zero field is called the diamagnetic cavity. For a further discussion of the diamagnetic cavity, see Lühr et al. [1985].

Information on the structure of the expanding ion cloud can be obtained from the propagation cutoff of the galactic radio noise. Early in the expansion phase the cutoff of the galactic radio noise is observed to be about a factor of two to three above the local electron plasma frequency. Our interpretation of this effect is that the ion cloud consists of a dense expanding shell with a depleted inner core, such as illustrated in Figure 3. Because the galactic radio noise is blocked by the expanding shell, the frequency range indicated by cross-hatching in Figure 3 is not accessible to the incoming radiation. This explains why the propagation cutoff observed by the IRM in the center of the cloud is above the local electron plasma frequency. The observed cutoffs suggest that the plasma density at the center of the cloud may be as much as a factor of ten lower than the density in the surrounding spherical shell.

The first evidence of a deviation from simple radial expansion is at 1233:15, where the density suddenly increases up to about 10^4 cm^{-3}. As can be seen from the bottom panel of Figure 2, this increase coincides almost exactly with the return of a strong magnetic field,

much stronger than the field that existed before the event. The interpretation of these effects is that the cloud has started to convect, thereby causing the spacecraft to enter a region of compressed plasma and magnetic field around the nose of the cloud. Although the cloud must eventually be carried downstream by the solar wind, ground optical observations [Rees et al., 1985] show that the initial motion is actually perpendicular to the solar wind flow. The approximate trajectory of the IRM relative to the diamagnetic cavity is shown by the dashed line in Figure 4. The motion perpendicular to the solar wind flow is believed to be a reaction to the acceleration of barium ions away from the cloud by the solar wind electric field. For a discussion of the cloud dynamics, see Haerendel et al. [1985]. Optical observations [Rees et al., 1985] indicate that the diamagnetic cavity expanded to a maximum radius of about 100 km about 2 to 3 minutes after the explosion. After this time the cloud began to dissipate and was rapidly swept downstream by the solar wind.

III. STATIC ELECTRIC FIELD

In addition to wave measurements the plasma wave instrument also provides measurements of the static electric field. The static electric field measurements obtained during the artificial comet experiment are shown in Figure 5. The top panel shows the E_x component of the electric field as detected in the low frequency waveform channel. This channel has a passband from 0.1 to 20 Hz. A nearly sinusoidal spin modulation signal, indicative of a static electric field, is clearly evident after 1232:00. Before the explosion, prior to 1232:00, a very strong signal is present that saturates the waveform channel. This signal is caused by the photoelectron cloud from the spacecraft. Because the electric antenna is relatively short, only 47.4m tip-to-tip, the spacecraft photoelectron cloud strongly affects the antenna potential in low density regions such as the solar wind. The much more dense plasma in the ion cloud shields the antenna from the photoelectron cloud, thereby permitting a measurement of the ambient field.

As can be seen, a small but easily detectable electric field is present in the diamagnetic cavity. This electric field increases from a few tenths of a mVolt/m shortly after entry to about 2 mVolt/m at the exit. As the spacecraft enters the plasma compression region at 1233:15 the electric field abruptly jumps up to about 2.5 to 3.0 mVolt/m, occasionally saturating the waveform channel. The electric

field stays at about this amplitude until about 1234:00, at which time the field starts to become noisy. At 1234:23 the noise suddenly becomes very intense, saturating the waveform channel. Further details of this intense noise will be discussed in Section VI. The electric field remains very noisy for about one minute, and then gradually returns to the strong photoelectron signal characteristic of the undisturbed solar wind.

To further analyze the static electric field signal it is useful to use a coordinate system called spacecraft-sun coordinates, denoted by a subscript "sc", which stands for spacecraft. In this coordinate system z_{sc} is parallel to the spacecraft spin axis, the sun is located in the x_{sc}, z_{sc} plane, and y_{sc} completes the right-hand system. This coordinate system is convenient because the measured electric field lies entirely in the x_{sc}, y_{sc} plane, and the unknown field is in the z_{sc} direction. At the time of the December 27, 1984, event the sun was about 4.6° above the x_{sc} axis, with the spin axis directed toward the south and tilted somewhat toward the dawn hemisphere.

Using a least-mean-square fitting procedure the magnitude and direction of the electric field have been determined in the x_{sc}, y_{sc} plane. These parameters are shown in the middle two panels of Figure 5. The angle Φ_E is the azimuthal direction of the electric field measured in the right-hand sense (toward $+y_{sc}$) from the $+x_{sc}$ axis. As can be seen, the angle ϕ_E starts out at about 45°, then increases to about 90°, where it remains for most of the event. Since the $+x_{sc}$ axis

is nearly along the spacecraft-sun line, the electric field is nearly perpendicular to the solar wind velocity.

Interpretation

The existence of a nearly steady electric field in the diamagnetic cavity is quite surprising since the electric field is usually expected to be zero in a highly conducting plasma with no magnetic field. We must therefore consider the possibility that the electric field signal is caused by some kind of spacecraft-related charging effect. It is well known that photoelectron emissions from the sunward side of the spacecraft can affect double-probe electric field measurements, particularly when the plasma density is very low. Indeed, such effects are observed before the explosion, when the electron density is only 8 cm^{-3}. However, immediately after the explosion the electron densities increase to 10^4 to 10^5 cm^{-3}. For these high densities double-probe electric field antennas usually give reliable results. Unfortunately, we have no conclusive test which can clearly determine if the electric field is real. For a real electric field the antenna voltage must vary sinusoidally as the spacecraft rotates. The observed signals provide a reasonably good fit to a sine wave. Probably the best indication that the electric field is real is the fact that similar fields were observed during the July 18, 1985, solar wind release, but no comparable field was observed during the two magnetotail barium releases on March 21 and May 13, 1985. The absence of an electric field during the magnetotail releases indicates that the electric field is somehow associated with the solar wind.

The fact that the electric field is nearly perpendicular to the solar wind velocity suggests a relationship to the convection electric field in the solar wind. To test this hypothesis we have taken the average magnetic field and solar wind velocity for two minutes before the event and computed $\vec{E} = -\vec{V}_{SW} \times \vec{B}$. The computed magnitude and direction, projected onto the x_{SC}, z_{SC} plane are $|\vec{E}| = 2.67$ mVolts/m and $\Phi_E = 85.4°$. These values are shown by the horizontal dashed lines in the middle two panels of Figure 5. As can be seen the direction and magnitude of the computed solar wind field are in excellent agreement with the observed field, particularly later in the event. The small deviations could easily be due to changes in the solar wind magnetic field during the event. The magnitude of the electric field is less than the solar wind field early in the event, but then recovers toward the solar wind value later in the event. By the time the spacecraft has entered the plasma compression region the electric field has returned almost completely to the preexisting solar wind value.

The simplest interpretation of these observations is that a substantial fraction of the solar wind electric field is able to penetrate into the diamagnetic cavity. This interpretation implies that the ion cloud is not able to generate the polarization charges necessary to shield out the external electric field. If a nearly uniform electric field of approximately 1 mV/m exists throughout the cloud, the potential difference across the cloud would be on the order of 100 Volts. How such a large potential difference could exist across the cloud without producing runaway electrons and large currents is not known.

Another possible interpretation is that the electric field is directed radially outward from the center of the cloud. Since motion of the cloud is initially perpendicular to the solar wind velocity, this would explain why the field is nearly perpendicular to the spacecraft-sun line. In this interpretation the field is entirely internal. The association with the solar wind field arises because the motion of the cloud is controlled by the external electric field. A radial electric field is, of course, necessary to confine the faster moving electrons to the ion cloud. The main issue is the magnitude of the field. To confine the electrons the potential difference between the center of the cloud and the outer boundary must be on the order of the thermal energy of the electrons. For the relatively low electron temperatures expected from photoionization, the potential difference should be only a few volts, which is much smaller than the potential difference implied by the electric field measurements. On the other hand, electrons with energies of several hundred eV were observed in the ion cloud, apparently caused by some external heating process [Haerendel et al., 1985]. It is possible that the observed electric field could be associated with the confinement of these more energetic electrons. This interpretation will require further study.

IV. WAVES INSIDE THE DIAMAGNETIC CAVITY

Next we describe the waves detected by the IRM inside the diamagnetic cavity. Generally the wave intensities in the diamagnetic cavity are quite low, much lower than in the solar wind. The wave intensities in the diamagnetic cavity are summarized in Figure 6, which shows the electric field strengths in sixteen frequency channels from 31 Hz to 178 kHz. The intensity scale for each channel is logarithmic and covers a dynamic range of 106 db, from about 0.5 μVolt/m to 100 mVolt/m. All sixteen frequency channels are sampled once every 0.125 seconds. Two relatively weak bands of noise can be seen in Figure 6 sweeping downward in frequency with increasing time, the first starting at about 5.62 kHz and sweeping down to about 1 kHz, and the second starting at about 562 Hz and sweeping down to about 178 Hz. Other than the high frequency electron plasma oscillations described in the previous section, which are not unique to the cavity, these are the only types of waves detected in the diamagnetic cavity. Further details of the two emission bands are given in Figure 7, which shows high resolution frequency-time spectrograms of the wideband waveform data. The upper band is shown in the top panel which covers the frequency range from 0 to 10 kHz, and the lower band is shown in the bottom panel which covers the frequency range from 0 to 1 kHz. The upper band, which is the narrowest, is almost exactly at the barium ion

plasma frequency, f_{pBa^+}. The ion plasma frequency can be computed by dividing the electron plasma frequency by the square root of the ion to electron mass ratio [Krall and Trivelpiece, 1973], which for barium ions is $\sqrt{m_{Ba}/m_e} = 501$. The relation of the upper band to the ion plasma frequency is further illustrated in Figure 8 which shows two electric field spectrums selected near the beginning and end of the event. As can be seen the center frequency of the upper band is almost exactly at the barium ion plasma frequency. The lower band is much broader and is about a factor of ten below the barium ion plasma frequency. The frequency of this band is not simply related to any known characteristic frequency of the plasma. The frequency variation of the lower band is also somewhat different than the upper band. The frequency initially increases, reaches a maximum of about 500 Hz at 1232:10, and then decreases slowly, more or less in proportion to the barium ion plasma frequency.

Close examination of the frequency-time spectrograms in Figure 7 shows that the two emission bands have considerable fine structure. Some of this fine structure is modulated at twice the spacecraft spin rate, which is one rotation every 4.4 seconds. Because the wideband receiver uses an automatic gain control, which tends to maintain a constant signal amplitude, the spin modulation is best studied by using intensity measurements from the 16-channel spectrum analyzer. The electric field intensities in the 562 Hz and 178 Hz channels are shown in Figure 9. These channels were selected to illustrate the spin modulation in the upper and lower bands, respectively. Both bands show a sharply defined peak in the electric field intensity when the antenna is nearly aligned along the spaeccraft-sun line.

Interpretation

The fact that the spin modulation pattern is sharply peaked has important implications. For long wavelength electrostatic waves a simple sinusoidal modulation should be observed. Since the modulation is clearly non-sinusoidal, the wavelength must be either short compared to the antenna length, thereby producing a non-sinusoidal response, or the emission intensity must be controlled by the spacecraft rotation. The latter would require a spacecraft-related source, such as photoelectrons or some type of wake effect.

A strong case can be made that the spin modulation pattern is caused by wavelengths shorter than the length of the antenna. The response of an electric dipole antenna to short wavelength electrostatic waves has been studied by Fuselier and Gurnett [1984], who showed that the measured antenna voltage is given by

$$v_m = \frac{L}{2} (E_\perp \cos \phi)\left[\frac{\sin x}{x}\right]^2 \qquad (1)$$

$$\text{where } x = \frac{k_\perp L}{4} \cos \phi \quad . \qquad (2)$$

The quantities $E_\perp$ and $k_\perp$ are the projections of the electric field and wave vector onto the spin plane, L is the tip-to-tip length of the antenna, and ϕ is the angle between $\vec{E}_\perp$ and $\vec{k}_\perp$. This equation assumes that the coupling of the antenna to the plasma is uniform along the length of the antenna. The short wavelength effects are contained in the sin x/x term. For long wavelengths, $\lambda >> L$, this term is unity,

and the antenna voltage has the usual sinusoidal modulation, as controlled by the cos ϕ term in Equation 1. For short wavelengths, $\lambda << L$, the sin x/x term produces a sharply peaked response near $x = 0$, or $\phi = 90°$ and 270°. This effect is illustrated in Figure 10, which shows a plot of the antenna gain factor, $G = (2V_m/LE_\perp)^2$, as a function of ϕ for $L/\lambda = 15$. As can be seen, the envelope of the antenna gain plot is very similar to the spin modulation pattern in Figure 9. The individual nulls are not evident in Figure 9. However, these nulls could easily be smeared out by a small spread in the wave normal direction, or by the finite time constant (0.05 sec) of the spectrum analyzer.

If the spin modulation pattern is due to short wavelength waves, then several conclusions can be made about the nature of these waves. First, the wave vector must be nearly perpendicular to the spacecraft-sun line. This conclusion follows from the antenna gain pattern, which has peaks at $\phi = 90°$ and 270°, and the intensity modulation, which has a maximum along the spacecraft-sun line. Second, the wave vectors must be confined to a narrow range of directions, otherwise the spin modulation pattern would not be sharply peaked. Third, the electric field strengths must be substantially larger than given in Figures 8 and 9, because the antenna gain is much less than one for short wavelengths. For example, if $L/\lambda = 15$, which gives a reasonable fit to the spin modulation pattern, the peak wave intensities would be a factor of 10^3 higher. The electric field strength of the upper and lower bands would then be about 0.5 mVolts/m and 1.0 mVolts/m, respectively.

Next we consider the possible plasma wave modes that could account for the emissions near and below the barium ion plasma frequency. For a plasma with no magnetic field, the only mode that can exist in this frequency range is the ion acoustic mode [Krall and Trivelpiece, 1973]. The dispersion relation for the ion acoustic mode is

$$\omega^2 = \frac{C_s^2 k^2}{1 + k^2 \lambda_D^2} \quad , \tag{3}$$

where k is the wave number, λ_D is the Debye length, and $C_s = (kT_e/m_i)^{1/2}$ is the ion acoustic speed. The characteristic scale length of the ion acoustic mode is the Debye length. For frequencies near the ion plasma frequency the wavelength is on the order of $2\pi\lambda_D$. The Debye length is determined by the electron temperature and electron density [Krall and Trivelpiece, 1973]. Since the electrons in the cloud are produced by photoionization, the electron temperature is determined by the solar ultraviolet spectrum and is expected to be about 10^4°K. For a representative electron density of 10^4 cm^{-3}, $2\pi\lambda_D$ is approximately 0.43 meters. This characteristic wavelength is much shorter than the antenna, which is 47 meters tip-to-tip. At frequencies below the ion plasma frequency, the wavelength varies inversely with the frequency, $\lambda = C_s/f$. For a representative electron density of 10^4 cm^{-3}, it is easily verified that the wavelength is less than 47 meters for all frequencies above 16 Hz. Since the frequencies observed in the

diamagnetic cavity are all above 16 Hz, the wavelengths are in all cases less than the antenna length. These results are consistent with our previous conclusions regarding the wavelength of these waves.

Next we consider the damping of the ion acoustic mode. Equation 3 shows that as the frequency increases the wavelength approaches zero as the frequency approaches the ion plasma frequency. Since some of the emissions have frequencies very close to the ion plasma frequency, these waves must have wavelength comparable to the Debye length. For wavelengths close to the Debye length, Landau damping can be quite important. As is well known [Krall and Trivelpiece, 1973], Landau damping is strongly controlled by the electron to ion temperature ratio, T_e/T_i. The damping is weak only if $T_e/T_i \gg 1$. Because the ion temperature is controlled by the chemical reaction that produced the barium cloud, the ions are expected to be very cold, not more than about 2,000°K. For an electron temperature of 10^4°K, T_e/T_i is approximately 5. This large electron to ion temperature ratio explains why the waves are not strongly damped.

Finally, we consider the instability responsible for generating the waves. At the present time we have no solid explanation for the origin of these waves. The ion acoustic mode can be driven unstable by a number of mechanisms, including currents, beams, and heat fluxes. Since the magnetic field is zero in the diamagnetic cavity, the current must also be zero. Therefore, it is unlikely that the waves are driven by currents. If an electron or ion heat flux exists across the cloud, the heat flux could drive an ion acoustic instability. Electrostatic

electron and ion heat flux instabilities have been discussed by Forslund [1970], and Gary [1978]. At present we have not yet investigated the plasma data in sufficient detail to comment on the existence of suitable heat fluxes to drive an ion acoustic instability. Finally, the solar wind proton beam streaming through the cloud could drive an ion acoustic instability. For a discussion of beam driven ion acoustic instabilities, see Lemons et al. [1979]. The solar wind beam mechanism has the desirable feature of generating waves at large angles to the solar wind velocity if $V_{sw} >> C_S$, which would explain why the wave vectors tend to be perpendicular to the spacecraft-sun line. Unfortunately, similar waves were also observed during the March 21 and May 13, 1985, barium releases in the magnetotail, which demonstrates that the waves are not uniquely related to the solar wind protons. It is possible that ion beams may also exist in the magnetotail, which could drive the instability. A full understanding of the origin of these waves will require further investigation.

V. WAVES AT THE CAVITY BOUNDARY

During both the entry and exit of the diamagnetic cavity, a broadband burst of noise was observed at the cavity boundary. This noise is responsible for the sharp spikes below about 3.11 kHz at 1232:00 and again at 1233:16 in Figure 6. Spectrums of these bursts, selected from the time of maximum intensity, are shown in Figure 12. The integrated broadband electric field strength is about 0.3 mVolts/m for the entry, and 0.4 mVolts/m for the exit, assuming an antenna gain of one (G = 1). In both cases the durations are very short, about 0.3 sec for the entry, and about 0.5 sec for the exit. Using the expansion speed of the cloud, estimated by Haerendel et al. [1985] to be 1.7 km/sec, the thickness of the unstable layer at the entry into the cavity is estimated to be about 500m. The corresponding thickness at the exit is more difficult to estimate because by then the expansion has slowed and the cloud has started to convect, but is probably on the order of a few km. As can be seen in Figure 12, the electrostatic noise corresponds almost exactly with the disappearance and appearance of the magnetic field at the boundaries of the diamagnetic cavity. In both cases the duration of the burst is comparable to the time scale of the magnetic field variation.

Interpretation

The close relationship of the broadband bursts of electrostatic noise to the magnetic field discontinuities strongly suggests that the noise is driven by the electron magnetization current that flows along the boundary of the diamagnetic cavity. The frequency range of the noise, near and below the barium ion plasma frequency, suggests that the noise may also consist of ion acoustic waves. As is well known, ion acoustic waves can be driven by a relative drift between the electrons and ions, such as must exist at the boundary of the diamagnetic cavity. When the electron temperature is much higher than the ion temperature, as is believed to be the case in the barium cloud, the threshold drift velocity for the ion acoustic instability is quite low, only a few times the ion thermal speed [Krall and Trivelpiece, 1973]. For barium ions at a temperature of 2,000°K, the ion thermal speed is only about 0.35 km/sec. Accordingly to the estimates of Haerendel et al. [1985] the electrons must be drifting relative to the ions at a velocity of about 13 km/s in order to account for the current at the cavity boundary. This drift velocity greatly the threshold drift velocity, thereby indicating that the ion acoustic mode should be unstable.

VI. WAVES ASSOCIATED WITH THE COMPRESSION REGION

The wave intensities outside of the diamagnetic cavity are shown in the 16-channel electric field plot of Figure 12. After leaving the diamagnetic cavity at 1233:16 and entering the plasma compression region the electric field intensities again drop to very low levels. Except for a few weak sporadic bursts the electric field intensities remain at a low level until about 1233:55, where they gradually begin to increase. At about 1234:23, near the outer boundary of the compression region the electric field intensities suddenly increase to very high levels, so high that they saturate some channels of the spectrum analyzer. After about 1235:10 the electric field intensities begin to decrease, gradually decreasing to the ambient solar wind level over a period of about one minute. Figure 13, which gives magnetic field spectral densities measured by the magnetometer, shows that this same interval, from about 1234:23 to 1235:10, is also characterized by very high magnetic noise levels. This region of very intense plasma wave noise will be referred to as a shock-like transition region. The similarity of this region to the transition region in the earth's bow shock has been previously pointed out by Gurnett et al. [1985] in an analysis of an AMPTE solar wind lithium release.

Representative electric field spectrums of the shock-like electric field noise are shown in Figure 13. The spectrums typically show a flat plateau at low frequencies, with a rapid decrease in intensity at frequencies above a few hundred Hz. Sometimes a slight peak or enhancement is evident near 100 Hz. At maximum intensity the broadband electric field strength, integrated over all the frequency channels, is 140 mVolts/m, and may be even higher because some of the channels are saturated. These electric field intensities are among the most intense ever recorded by a space plasma wave experiment. Wideband spectrograms of the electric field waveform, illustrated in Figure 15, show that the spectrum is relatively featureless. In particular, there is no evidence of emissions near the electron cyclotron frequency, f_{ce}, or the lower-hybrid resonance frequency, $f_{LHR} = (f_{ce}f_{ei})^{1/2}$. The lower-hybrid frequency should be in the range from a few Hz to a few tens of Hz, depending on the plasma composition. Also, no evidence of spin modulation can be seen in the electric field intensity, indicating that the waves responsible for the noise are generated over a broad range of wave normal directions.

Proceeding farther upstream another type of higher frequency electric field noise can be seen in Figure 12 starting at about 1235:05. Two representative spectrums of this upstream noise are shown in Figure 16. The spectrum of this noise is characterized by a broad peak extending from about 3 to 30 kHz, somewhat below the electron plasma frequency. After the initial sharp onset, the center frequency and intensity of this noise tend to decrease with increasing time.

Occasionally a sharp peak can be seen in the spectrum, as at 1235:40 in Figure 16. This peak is believed to be at the local electron plasma frequency.

Interpretation

The existence of the intense electrostatic noise near the outer boundary of the compression region raises an important question as to whether this noise and the related plasma effects are caused by a collisionless shock. This question was first considered by Gurnett et al. [1985] in the interpretation of the AMPTE solar wind lithium releases and was motivated by the fact that the electrostatic noise has a spectrum very similar to the electrostatic noise observed in the earth's bow shock [Fredricks et al., 1968, 1970a,b; Rodriguez and Gurnett, 1975; Gurnett, 1985]. If the effects observed upstream of the artificial comet are to be interpreted as a shock then certain basic conditions must be satisfied. The first requirement for a shock is that the plasma must have a component of flow across the discontinuity. It is quite clear that that solar wind plasma flows continuously through this region. This fact is illustrated in the top panel of Figure 17 which shows an energy-time spectrogram of ions arriving from the direction of the sun. The dark band across the spectrogram at an energy of about 200 to 500 eV is due to solar wind protons. As can be seen, the flux of solar wind protons is essentially continuous through the entire event. The second requirement for a shock is that the plasma flow velocity must decrease, and that the plasma density and magnetic field must increase. Figure 2 clearly shows that the plasma

density and magnetic field increase in the region where the intense electrostatic noise occurs. The flow speed of the solar wind protons is shown in the second panel from the bottom in Figure 17. This plot shows that a large reduction in the solar wind proton speed occurs in the region of intense wave activity. The reduction in the flow velocity is probably even more pronounced than indicated because the plasma instrument does not detect the bulk of the barium ions, which are nearly at rest with respect to the spacecraft. The third and final requirement for a shock is that the entropy must increase as the plasma flows across the shock. Whether this condition is satisfied cannot be answered quantitatively because the plasma instrument does not have sufficient resolution to accurately measure the plasma temperature. However, as can be seen in the middle and bottom panels of Figure 17, the plasma is definitely being heated in the region where the noise occurs. This heating provides strong qualitative evidence that the entropy is increasing. Although it is not certain that the highly turbulent region upstream of the ion cloud is a shock, it certainly has many features similar to a shock.

Next we consider the origin of the intense electrostatic noise in the shock-like transition region. Our present view is that the noise is caused by an ion beam-plasma interaction between the nearly stationary barium ions and the rapidly moving solar wind protons. The essential elements of this instability were discussed by Gurnett et al. [1985] in the analysis of the AMPTE solar wind lithium releases. The reduced one-dimensional distribution function assumed in this model is

shown in Figure 18. Because the barium ions are born at rest, these ions are represented by a Maxwellian centered on zero velocity. The barium ions are assumed to be very cold, only 2×10^3°K. The solar wind protons are represented by a Maxwellian centered on the solar wind velocity, V_{sw}, which is taken to be 500 km/sec. The solar wind proton temperature is assumed to be hotter, about 10^5°K. Two classes of electrons must be considered, relatively cold, $\sim 10^4$°K, electrons from the photoionization of barium, and much hotter, $\sim 5 \times 10^5$°K, solar wind electrons, which have been heated somewhat in the vicinity of the cloud. Both classes of electrons are represented by Maxwellians and are assumed to be drifting at a velocity, V_d, that is adjusted such that the net current in the plasma is zero. This last condition is based on the fact that the magnetic field measurements show that the net current in the plasma is small compared to the current contributed by the solar wind protons.

Two types of beam-plasma instabilities can occur in this type of plasma, one with phase velocities between the barium ions and the electrons, $0 < \omega/k < V_d$, and the other between the electrons and the solar wind protons, $V_d < \omega/k < V_{sw}$. Of these, only the instability associated with the barium ions is important. The reason is that the instability is very similar to an ion acoustic instability and is strongly influenced by the electron to ion temperature ratio. Because the barium ions are much colder than the protons, the instability associated with the barium ions has a much lower threshold. The growth rate of the ion beam-plasma instability is strongly controlled by the

relative density of the barium ions and the protons. Instability only occurs if the two ion species have somewhat similar plasma frequencies. Otherwise, the instability associated with the minority ion disappears because the "beam" density is too low, and the instability associated with the majority ion disappears because the drift velocity with respect to the electrons is too low. This density dependence explains why the electrostatic noise is only observed near the outer boundary of the ion cloud. It is only in this region (see Figure 2) that the barium ion and proton densities are sufficiently similar for the instability to occur.

Because the ion beam-plasma instability has been previously analyzed for a solar wind lithium release [Gurnett et al., 1985], we will only present a summary of the corresponding analysis for the December 27 barium release. Figure 19 shows the marginal stability boundary ($\gamma = 0$) for propagation parallel to the solar wind velocity plotted as a function of the frequency and the barium ion to proton density ratio. This analysis uses the previously mentioned temperatures and velocities and assumes that the cold photoelectron density is equal to the barium ion density. Although the cold photoelectron density cannot be directly measured, it has been previously shown [Gurnett et al., 1985] that the results are relatively insensitive to this parameter. The marginal stability plot shows that electrostatic waves are unstable for frequencies up to about 350 Hz, and for barium ion to proton density ratios from about 2.2×10^{-2} to 2.6×10^{2}. The observed frequency range of the electrostatic noise, up to a few hundred Hz (see

Figure 14), and the onset of the electrostatic noise, at a density ratio of $N_{Ba}^{+}/N_p \approx 10^2$ (see Figures 2 and 12), are in good agreement with the predictions of the model. Unfortunately, the lower bound for the density ratio cannot be compared because the barium ion density cannot be accurately determined beyond about 1234:30.

Detailed growth rate calculations for a representative set of parameters are shown in the bottom panel of Figure 20. These calculations predict growth rates up to about 10 sec^{-1}. These growth rates are more than adequate to generate intense waves in the time for a wave to propagate through the transition region. The top panel of Figure 20 shows that the wavelengths produced are very short ($k\lambda_D \sim 0.1$). These wavelengths are much shorter than the thermal electron cyclotron radius, which justifies ignoring the static magnetic field. Although the basic model is one-dimensional, the results can be easily extended to waves propagating at an arbitrary angle [Krall and Trivelpiece, 1973], in which case growth occurs over a large range of wave normal directions, in agreement with the observations.

Before concluding the analysis of the ion beam-plasma instability, it is useful to discuss the possible role of barium ions accelerated by the solar wind electric field. The second panel from the top in Figure 17 shows two distinct ion populations that are well separated from the solar wind protons. One of these components, from about 1234:10 to 1236:00, is believed to consist of barium ions that have been accelerated by the solar wind electric field [Haerendel et al., 1985]. The energy of this component increases with increasing time,

starting at a few tens of eV and extending to over 1 keV. The energy is believed to increase because the path length available for acceleration increases as the cloud moves away from the spacecraft. As can be seen by comparing with Figure 12, the accelerated barium ions are observed over almost exactly the same interval as the intense electrostatic noise. This relationship is believed to be largely coincidental, because barium ions with even higher densities must be present before 1234:10, but at energies too low to be detected. Also, even at energies of several keV the barium velocities are still much less than the solar wind velocity. Therefore, the barium ion velocity is small and should have little effect on the stability analysis. Furthermore, the acceleration is nearly perpendicular to the solar wind velocity, which further diminishes the effect on the reduced one-dimensional distribution function.

In addition to the intense electrostatic noise, the magnetic noise and the high frequency electrostatic noise also requires analysis. At the present time we have not undertaken a detailed analysis of either of these types of noise. It is our impression that the magnetic noise may be due to an electromagnetic ion beam instability, possibly similar to the instability responsible for low frequency ULF waves upstream of the earth's bow shock [Gary et al., 1981; Winske and Leroy, 1984] with the barium ions playing the same role as upstream ion beams. As discussed earlier, the high frequency electrostatic noise appears to be associated with the electron plasma frequency. It seems likely that these waves are electron plasma oscillations which are downshifted in

frequency, similar to the waves described by Fuselier et al. [1985] upstream of the earth's bow shock. For beam energies near the electron thermal speed the frequency range of the Langmuir mode is broadened and shifted downward in frequency below the electron plasma frequency. At present it is not known whether an appropriate beam is present or not. The electron energy spectrum in the middle panel of Figure 17 does not show any evidence of such a beam, although Rodgers et al. [1985] did detect an electron beam at the UKS spacecraft during this same interval. It is also possible that barium ions upstream of the cloud could provide a suitable "beam" for driving this instability, when viewed from the solar wind frame of reference.

VII. CONCLUSIONS

The plasma waves and electric fields observed during the artificial comet experiment showed many similarities, and several notable differences with the previous solar wind lithium releases. The electron density profile obtained during the barium release was much clearer and better defined, with a substantially higher peak density. This is due to the more rapid ionization of barium, which produced a much more dense ion cloud. The higher density and longer duration also provided a much better determination of the static electric field in the diamagnetic cavity. The static electric field measurements show the existence of an electric field in the diamagnetic cavity. This field is in the same direction as the solar wind convection electric field, which suggests that the solar wind field is able to partially penetrate into the cloud. How such a large electric field can exist in an essentially collisionless plasma without causing large disruptive effects is not known. The observation of an electrostatic emission line at the barium ion plasma frequency is a new effect that was largely unanticipated. Subsequent analysis of the lithium releases [Häusler et al., 1986] reveals that a similar emission line was probably also present at the lithium ion plasma frequency, although the emission is not nearly as clear or well defined as in the barium release. Analysis of the spin modulation of these emissions strongly

indicates that this noise is caused by waves with very short wavelengths, probably ion acoustic waves. The free energy source for these waves still has not been clearly established, although the direction of propagation suggests that they may be driven by solar wind protons streaming through the ion cloud. Outside of the diamagnetic cavity the most notable plasma wave effect was the very intense electrostatic noise detected near the outer boundary of the plasma compression region. This noise is similar to the noise observed upstream of the lithium cloud, but more intense. The question again arises as to whether this noise is indicative of a shock-like interaction between the ion cloud and the solar wind. Although it is not certain that this highly turbulent region is a shock, it certainly has many characteristics similar to a shock. As in the lithium release it seems reasonably certain that the intense electrostatic noise is caused by a beam-plasma interaction between the nearly stationary barium ions and the rapidly moving solar wind protons. The possible role of this noise in heating the plasma needs further investigation.

This experiment showed many interesting new plasma effects associated with neutral gas injections in rapidly moving plasmas. Some of these effects, particularly the shock-like interaction on the upstream side of the ion cloud are expected to be relevant to natural comets, where similar types of instabilities are expected to occur.

ACKNOWLEDGEMENTS

We wish to thank Mr. Gracen Joiner of the Office of Naval Research (ONR) for his invaluable support, without which we would not have been able to carry out this project. We also thank Mr. D. Odem of the University of Iowa, Mr. W. B. Harbridge of Aerospace Corporation, and Mr. K. Gnaiger and Mr. F. Eberl of the Max-Planck-Institut für extraterrestrische Physik for valuable technical support. The research at the University of Iowa was supported by ONR contracts N00014-82-K-0183 and N00014-85-K-0404, and NASA grants NGL-16-001-002 and NGL-16-001-043. The research at the Aerospace Corporation was supported in part by the ONR and in part by the U. S. Air Force Systems Commands Space Division under contract F04701-84-C-0085. The research at The University of Washington was supported by ONR contracts N00014-84-K-0160.

REFERENCES

Biermann, L., R. Lüst, Rh. Lüst and H. U. Schmidt, Zur Untersuchung des interplanetaren Mediums mit Hilfe künstlich eigenbrachter Ionenwolken, Z. F. Astrophysik, 53, 226, 1961.

Forslund, D. W., Instabilities associated with heat conduction in the solar wind and their consequences, J. Geophys. Res., 75, 17, 1970.

Fredricks, R. W., F. W. Coroniti, C. F. Kennel and F. L. Scarf, Fast-resolved spectra of electrostatic turbulence in the earth's bow shock, Phys. Rev. Lett., 24, 994, 1970a.

Fredricks, R. W., G. M. Crook, C. F. Kennel, I. W. Green, and F. L. Scarf, OGO 5 observations of electrostatic turbulence in bow shock magnetic structures, J. Geophys. Res., 75, 3751, 1970b.

Fredricks, R. W., C. F. Kennel, F. L. Scarf, G. M. Crook, and I. M. Green, Detection of electric-field turbulence in the earth's bow shock, Phys. Rev. Lett., 21, 1761, 1968.

Fuselier, S. A., and D. A. Gurnett, Short wavelength ion waves upstream of the earth's bow shock, J. Geophys. Res., 89, 91, 1984.

Fuselier, S. A., D. A. Gurnett and R. J. Fitzenreiter, The downshift of electron plasma oscillations in the electron foreshock region, J. Geophys. Res., 90, 3935, 1985.

Gary, S. P., Electrostatic heat flux instabilities, J. Plasma Phys., 20, 47, 1978.

Gary, S. P., J. T. Gosling and D. W. Forslund, The electromagnetic ion beam instability upstream of the earth's bow shock, J. Geophys. Res., 86, 6691, 1981.

Gurnett, D. A., Plasma waves and instabilities, in Collisionless Shocks in the Heliosphere, ed. by R. Stone and B. Tsurutani, AGU, Washington, 207, 1985.

Gurnett, D. A., R. R. Anderson, B. Häusler, G. Haerendel, O. H. Bauer, R. A. Treumann, H. C. Koons and R. H. Holzworth, Plasma waves associated with the AMPTE artificial comet, Geophys. Res. Lett., 11, 851, 1985.

Haerendel, G., Plasma confinement and interaction experiment, Active Experiments in Space, ESA Report SP-196, 337, 1983.

Haerendel, G., and R. Lüst, Artificial plasma clouds in space, Sci. American, 219, 80, 1968.

Haerendel, G., R. Lüst and E. Rieger, Motion of artificial ion clouds, Planet. Space Sci., 15, 1, 1967.

Haerendel, G., Interaction of lithium clouds with the interplanetary medium, J. Geophys. Res., submitted, 1985.

Haerendel, G., G. Paschmann, W. Baumjohann, and C. W. Carlson, Dynamics of the AMPTE artificial comet, Science, submitted, 1985.

Häusler, B., R. R. Anderson, D. A. Gurnett, H. C. Koons, R. H. Holtzworth, O. H. Bauer, R. Treuman, K. Gnaiger, D. Odem, W. B. Harbridge, and F. Eberl, The plasma wave instrument onboard the AMPTE-IRM spacecraft, IEEE Trans. Geosci. Electronics, GE-23, 267, 1985a.

Häusler, B., L. J. Wolliscroft, R. R. Anderson, D. A. Gurnett, R. H. Holzworth, H. C. Koons, O. H. Bauer, G. Haerendel, R. A. Treumann, P. J. Christiansen, A. G. Darbyshire, M. P. Gough, S. R. Jones, A. J. Norris, H. Lühr, and N. Klöcker, Plasma waves observed by the IRM and UKS spacecraft during the AMPTE solar wind lithium releases: Overview, J. Geophys. Res., accepted, 1985.

Krimigis, S. M., G. Haerendel, R. W. McEntire, G. Paschmann, and D. A. Bryant, The Active Magnetostpheric Particle Tracer Explorers (AMPTE) Program, EOS, 63, 843, 1982.

Krall, N. A., and A. W. Trivelpiece, Principles of Plasma Physics, McGraw-Hill, N. York, 473, 1973.

Lemons, D. S., J. R. Asbridge, S. J. Bame, W. C. Feldman, S. P. Gary, and J. T. Gosling, The source of electrostatic fluctuations in the solar wind, J. Geophys. Res., 84, 2135, 1979.

Lühr, H., N. Klöcker, W. Oelschlägel, B. Häusler, and M. Acuña, The IRM magnetometer, IEEE Trans. Geosci. Electron., GE-23, 259, 1985a.

Lühr, H., N. Klöcker, D. J. Southwood, M. W. Dunlop, W. A. C. Mier-Jedrzejowicz, R. P. Rijnbeek, M. Six, B. Häusler and M. Acuña, In-situ magnetic field observations of AMPTE's artificial comet, Science, submitted, 1985.

Paschmann, G., H. Loidl, P. Obermayer, M. Ertl, R. Laborenz, N. Sckopke, W. Baumjohann, C. W. Carlson, and D. W. Curtis, The plasma instrument on AMPTE IRM, IEEE Trans. Geosci. Electron., GE-23, 262, 1985.

Rees, D., T. J. Hallinan, H. C. Steinbeck-Nielsen, M. Mendillo, J. Baumgardner, and P. A. Bernhardt, Optical observations of the AMPTE artificial comet release from the northern hemisphere, Science, submitted, 1985.

Rodgers, D. J., A. J. Coates, A. D. Johnstone, M. F. Smith, D. A. Bryant, D. S. Hall, and C. P. Chaloner, UKS plasma measurements near the AMPTE artificial comet, Science, submitted, 1985.

Rodriguez, P., and D. A. Gurnett, Electrostatic and electromagnetic turbulence associated with the earth's bow shock, J. Geophys. Res., 80, 19, 1975.

Scarf, F. L., R. W. Fredricks, L. A. Frank and M. Neugebauer, Nonthermal electrons and high frequency waves in the upstream solar wind: 1. Observations, J. Geophys. Res., 76, 5162, 1971.

Valenzuela, A., G. Haerendel, H. Föppl, F. Melzner, H. Neuss, E. Rigger, J. Stoecker, O. Bauer, H. Höfner, and J. Loidl, the artificial comet experiments, Science, submitted, 1985.

Winske, D., and M. M. Leroy, Diffuse ions produced by electromagnetic ion beam instabilities, J. Geophys. Res., 89, 2673, 1984.

FIGURE CAPTIONS

Figure 1. A frequency-time spectrogram from the high frequency sweep-frequency receiver. The dense plasma cloud formed by the explosion at 1232:00 blocked the galactic and terrestrial radio noise and produced depressed noise intensities for about two minutes as the cloud expanded over the spacecraft. The electron number density can be determined from the electron plasma oscillation line, which is at the local electron plasma frequency, f_{pe}.

Figure 2. The top panel shows the electron number density as obtained from the electron plasma oscillation line in Figure 1. The bottom panel shows the magnetic field, $|\vec{B}|$, from the magnetometer. Two distinct regions can be identified: the diamagnetic cavity where $|\vec{B}| = 0$, and the plasma compression region where the plasma density and magnetic fields are temporarily enhanced by the interaction with the solar wind.

Figure 3. The fact that the galactic radio noise cutoff is above the local electron plasma frequency suggests that the ion cloud is initially expanding as a dense shell with a

depleted inner core. The depletion produces a gap (cross-hatched) between the galactic cutoff and the local plasma frequency, f_{pe}.

Figure 4. A schematic diagram showing the diamagnetic (B = 0) cavity, the magnetic field lines draped around the cavity, and the compressed plasma upstream of the cavity. The diamagnetic cavity moved in such a way that the IRM followed the trajectory shown by the dashed line.

Figure 5. The quasi-static electric field measurements obtained from the low frequency waveform channel. The sinusoidal modulation in the upper panel is caused by the spacecraft rotation. This modulation can be analyzed to give the magnitude, $|\vec{E}|$, and direction, Φ_E, of the electric field projected onto the spin plane of the antenna.

Figure 6. An expanded 16-channel plot showing the electric field intensities in the diamagnetic cavity. Two distinct emission lines can be seen in the cavity: an upper band near the barium ion plasma frequency, f_{pBa^+}, and a lower band well below f_{pBa^+}. Abrupt broadband bursts of noise can also be seen at the boundaries of the diamagnetic cavity.

Figure 7. High resolution frequency-time spectrograms of the wideband data showing details of the two emission bands observed in the diamagnetic cavity. The upper band is almost exactly at the barium ion plasma frequency, f_{pBa^+}.

Figure 8. Selected electric field spectral density plots showing the intensity of the two emission bands observed in the diamagnetic cavity. The barium ion plasma frequency, f_{pBa^+}, was computed from the electron plasma oscillation line in Figure 1.

Figure 9. Expanded intensity plots showing the spin modulation of the two emission bands observed in the diamagnetic cavity. In both cases the intensity is sharply peaked as the antenna axis is aligned approximately along the spacecraft-sun line.

Figure 10. A plot of the antenna gain as a function of the angle, ϕ, between the wave vector and the antenna axis for an electrostatic wave with a wavelength, λ, short compared to the antenna length, L. The sharply peaked response is believed to account for the sharply peaked spin modulation pattern in Figure 9.

Figure 11. Electric field spectral density plots showing the spectrum of the noise observed at the boundaries of the diamagnetic cavity. This noise is believed to be caused by ion acoustic waves driven by the electron current flowing along the cavity boundary.

Figure 12. A 16-channel electric field intensity plot showing the intense shock-like noise observed near the outer boundary of the plasma compression region, and the broadband electron plasma oscillations in the more distant upstream region.

Figure 13. A plot of the magnetic field spectral density near the plasma compression region. The intense magnetic noise occurs in approximately the same region as the intense shock-like electrostatic noise.

Figure 14. Selected electric field spectrums of the intense shock-like electrostatic noise. Most of the power in this noise is concentrated at frequencies below a few hundred Hz.

Figure 15. Wideband electric field spectrograms of the intense shock-like electric field noise. The spectrum of the shock-like noise is relatively featureless, with no evidence of lines near either the electron cyclotron frequency or the lower hybrid resonance frequency.

Figure 16. Electric field spectrums showing the spectrum of the broadband electron plasma oscillations observed in the upstream region. The spectrum of these emissions is very broad, and is shifted downward somewhat below the electron plasma frequency.

Figure 17. Energy-time spectrograms and selected bulk parameters from the plasma instrument. The top panel shows that the solar wind proton stream was observed continuously throughout the event. The ions detected in the anti-sunward viewing hemisphere from about 1234:10 to 1236:00 are believed to be barium ions accelerated by the solar wind electric field. These ions are observed during the same time that the intense shock-like noise is observed.

Figure 18. A schematic illustration of the reduced one-dimensional velocity distribution believed to be responsible for the intense shock-like electric field noise. The basic instability is believed to occur at phase velocities, ω/k, between the barium ions and the electrons. The electrons are assumed to drift at a velocity V_d such that the net current is zero.

Figure 19. The marginal stability boundary ($\gamma = 0$) and maximum growth rate (γ_{max}) of the ion beam-plasma instability as a function of frequency and the barium ion to proton density ratio, N_{Ba^+}/N_p. Note that the instability only occurs for a limited range of N_{Ba^+}/N_p. This explains why the noise is confined to a relatively limited region near the outer boundary of the plasma compression region.

Figure 20. The growth rate, γ, and wave number, k, of the ion beam-plasma instability as a function of frequency for a representative set of parameters. The maximum growth rate in this case occurred at a frequency of 90 Hz, and a wave number of $k\lambda_D \approx 0.1$.

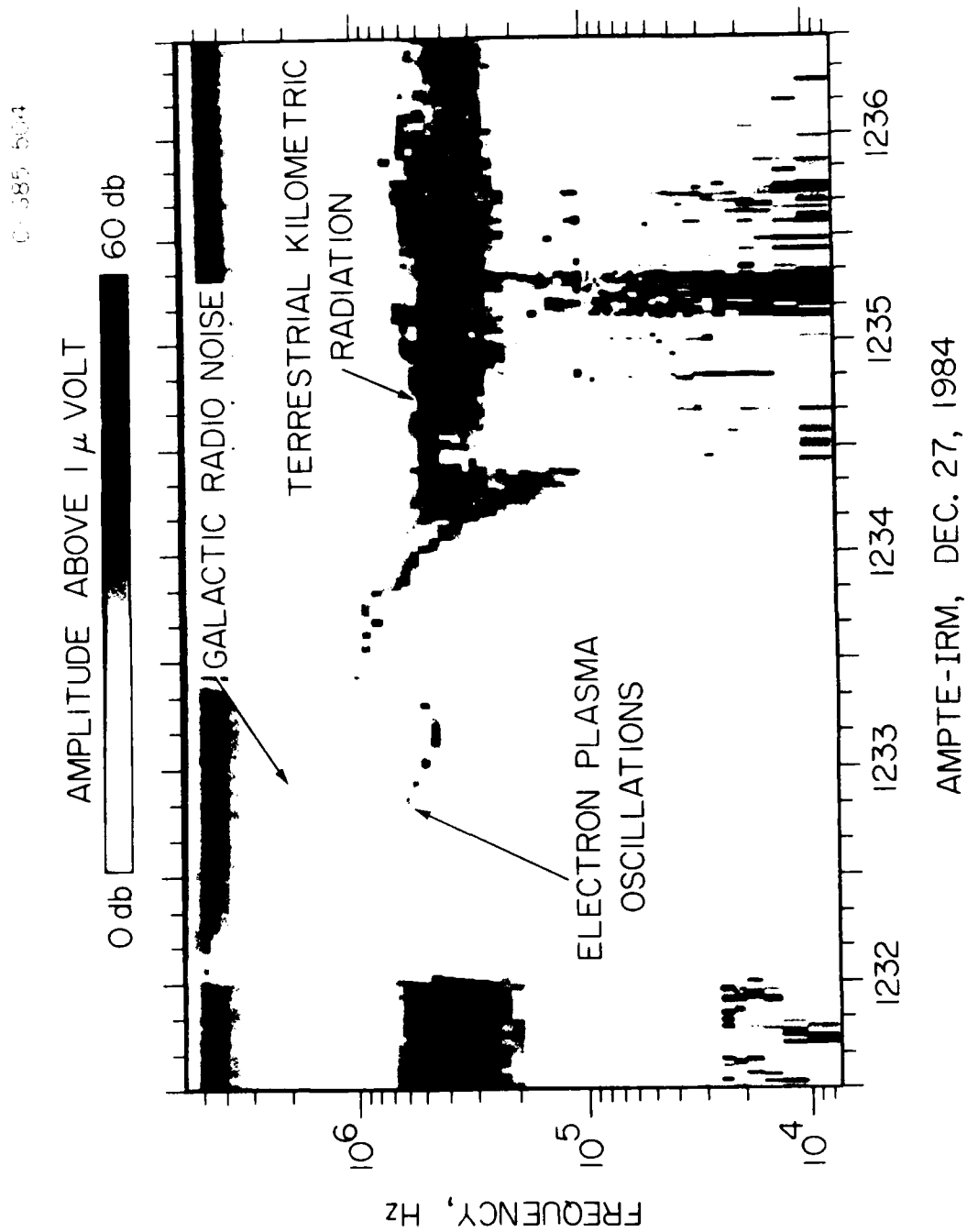
AMPLITUDE ABOVE 1 μ VOLT
0 db
60 db
GALACTIC RADIO NOISE
TERRESTRIAL KILOMETRIC RADIATION
ELECTRON PLASMA OSCILLATIONS
FREQUENCY, Hz
10^6
10^5
10^4
1232
1233
1234
1235
1236
AMPTE-IRM, DEC. 27, 1984

Figure 1

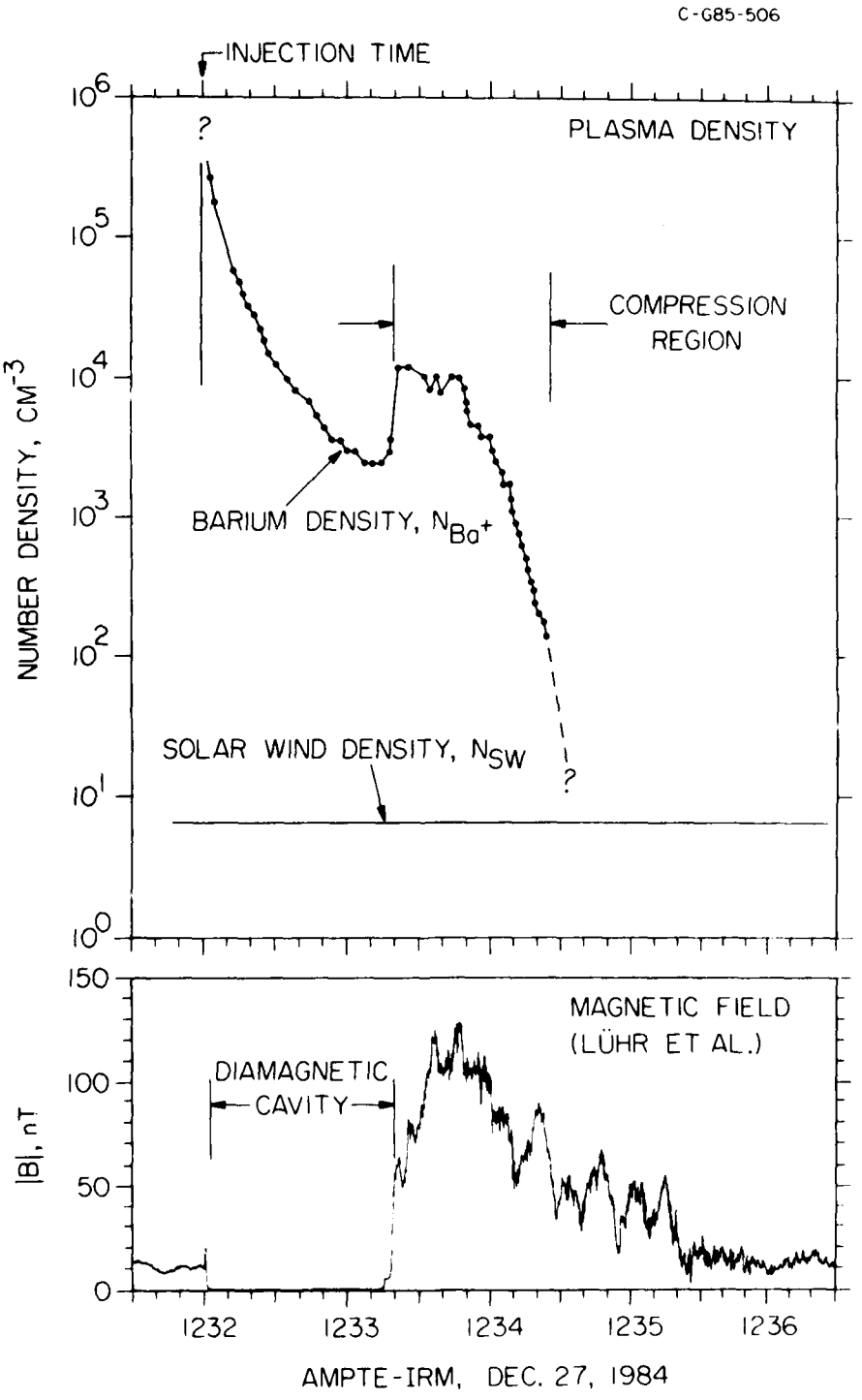
C-G85-506
INJECTION TIME
PLASMA DENSITY
?
COMPRESSION
REGION
BARIUM DENSITY, N_{Ba^+}
SOLAR WIND DENSITY, N_{SW}
?
NUMBER DENSITY, CM^{-3}
10^6
10^5
10^4
10^3
10^2
10^1
10^0
MAGNETIC FIELD
(LÜHR ET AL.)
DIAMAGNETIC
CAVITY
|B|, nT
150
100
50
0
1232
1233
1234
1235
1236
AMPTE-IRM, DEC. 27, 1984

Figure 2

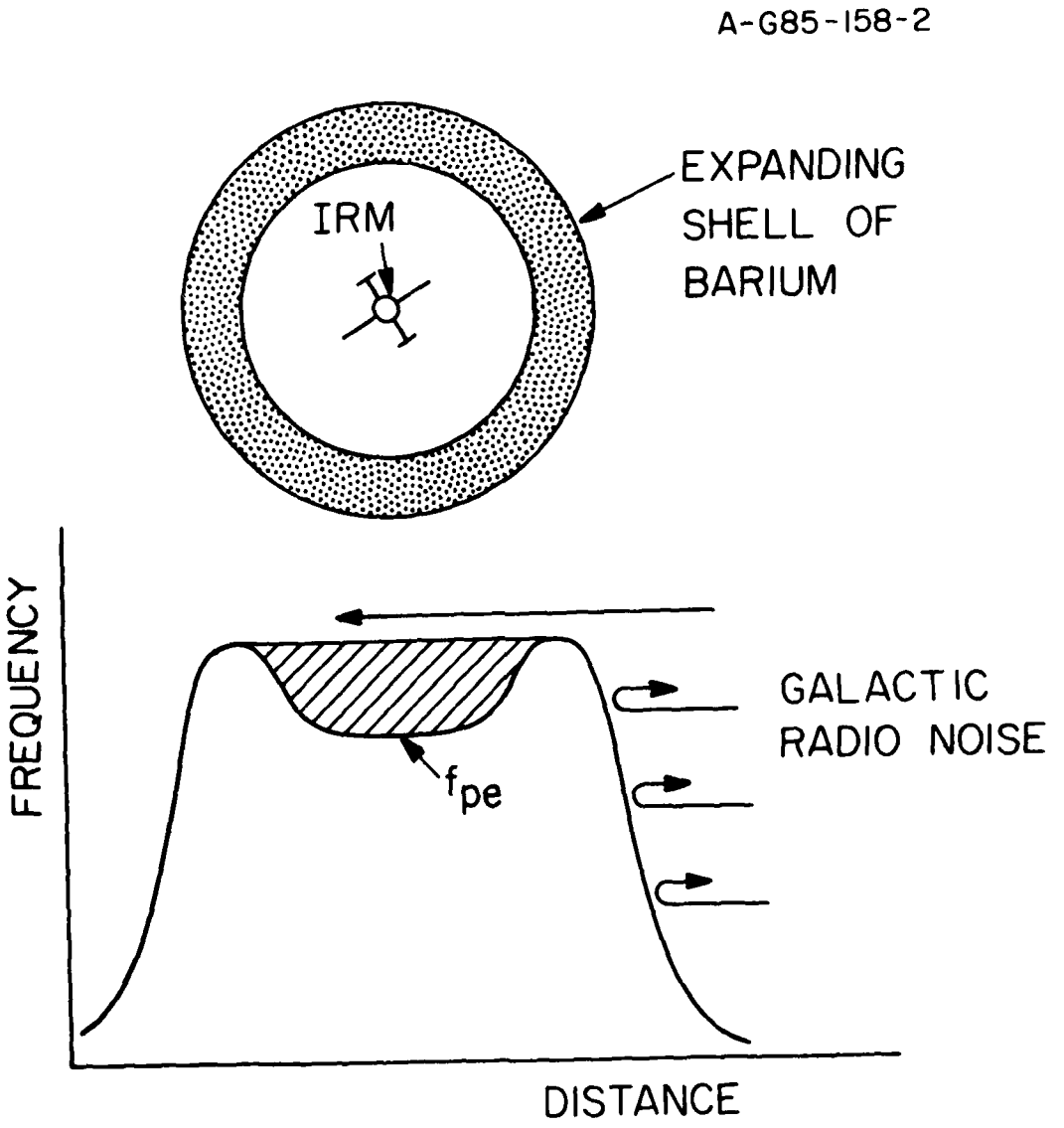
A-G85-158-2
IRM
EXPANDING
SHELL OF
BARIUM
FREQUENCY
f_{pe}
GALACTIC
RADIO NOISE
DISTANCE

Figure 3

A-G85-543-1

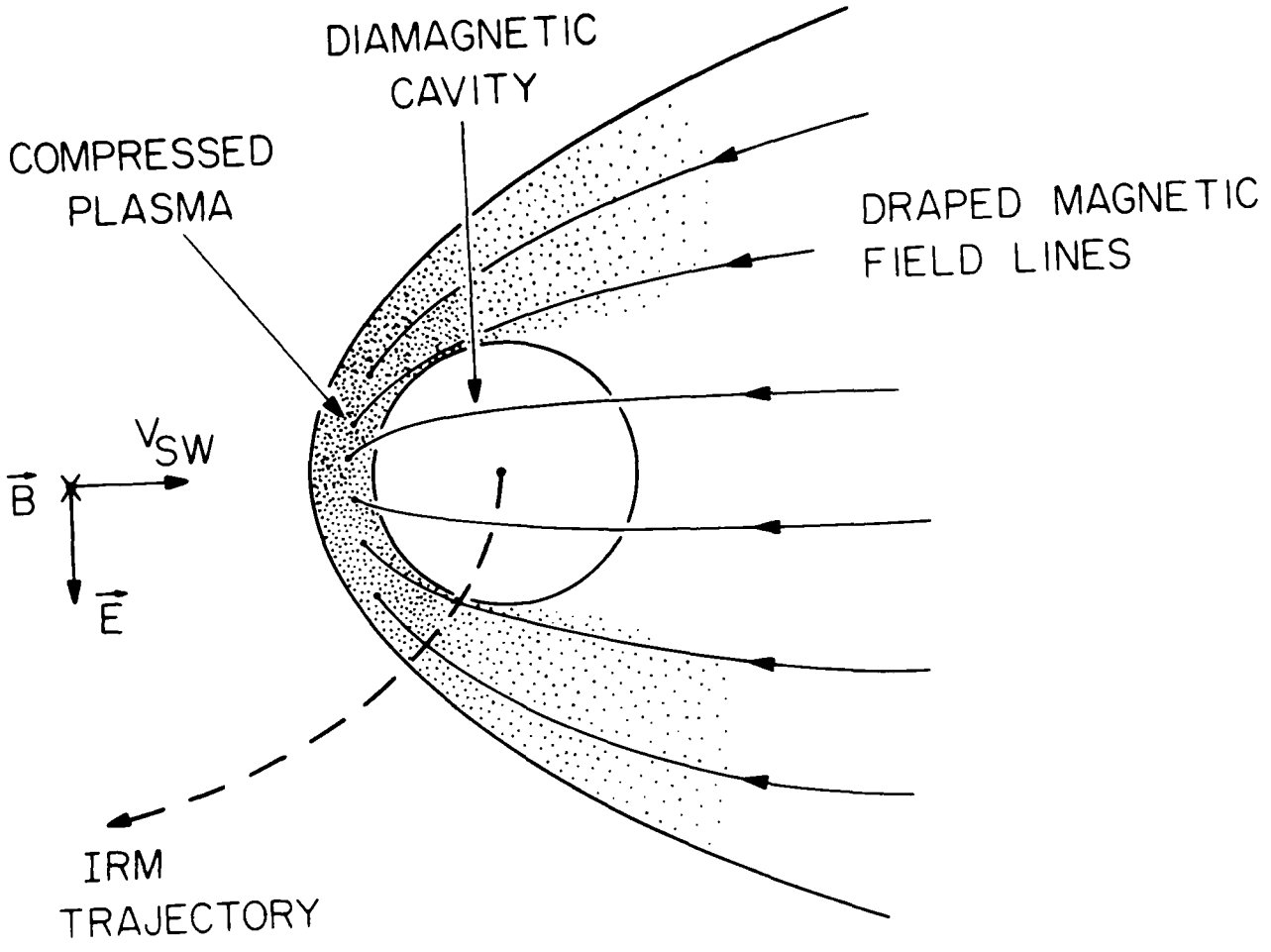

Figure 4

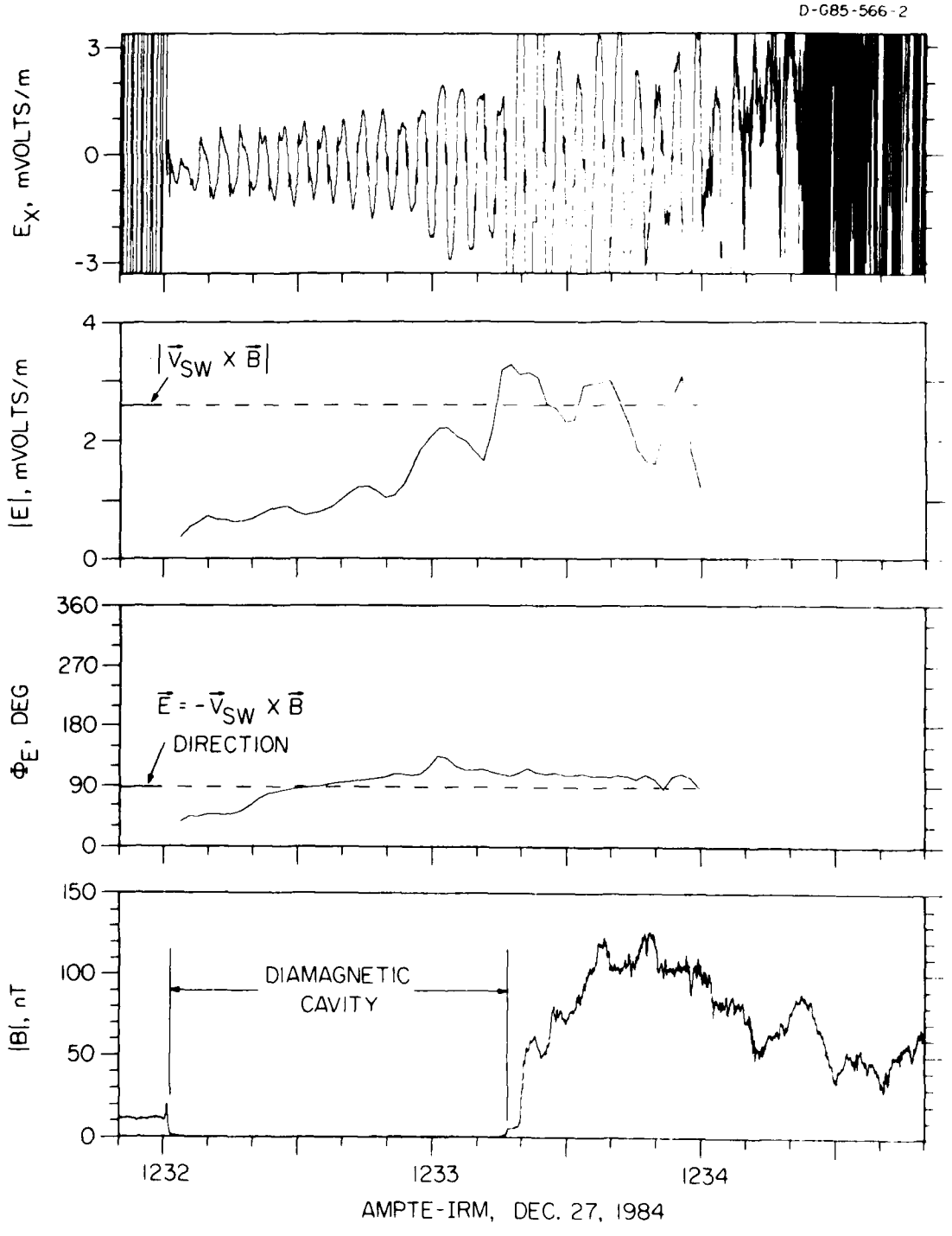
D-G85-566-2
E_X, mVOLTS/m
3
0
-3
|E|, mVOLTS/m
4
2
0
$|\vec{V}_{SW} \times \vec{B}|$
Φ_E, DEG
360
270
180
90
0
$\vec{E} = -\vec{V}_{SW} \times \vec{B}$
DIRECTION
|B|, nT
150
100
50
0
DIAMAGNETIC
CAVITY
1232
1233
1234
AMPTE-IRM, DEC. 27, 1984

Figure 5

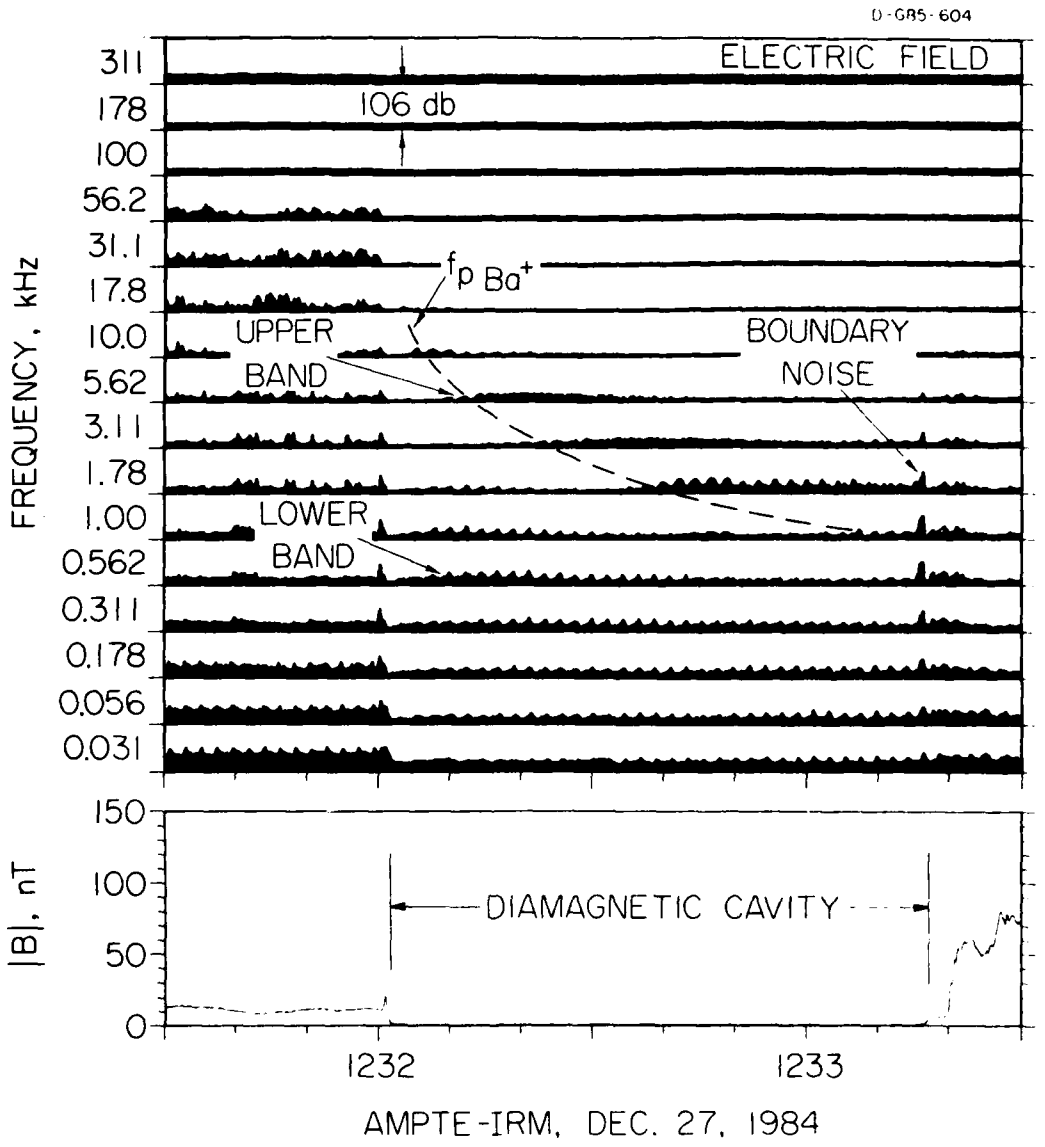
D-685-604
ELECTRIC FIELD
106 db
311
178
100
56.2
31.1
17.8
10.0
5.62
3.11
1.78
1.00
0.562
0.311
0.178
0.056
0.031
FREQUENCY, kHz
f_p Ba^+
UPPER
BAND
BOUNDARY
NOISE
LOWER
BAND
150
100
50
0
|B|, nT
DIAMAGNETIC CAVITY
1232
1233
AMPTE-IRM, DEC. 27, 1984

Figure 6

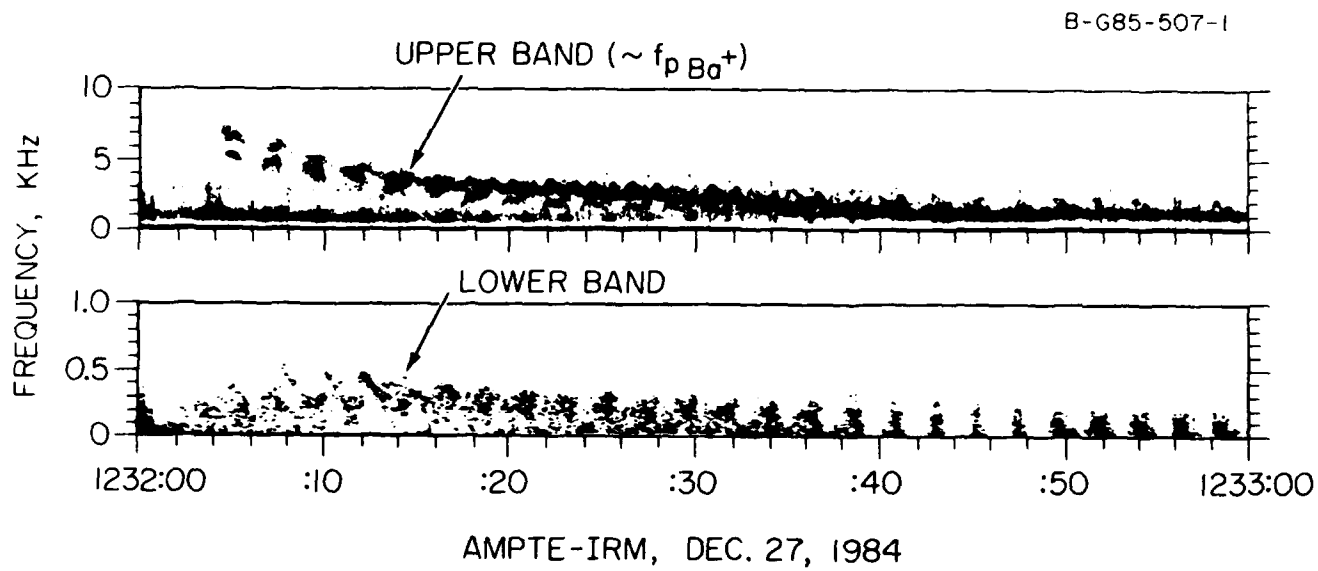
B-G85-507-1
UPPER BAND (~ $f_{p\,Ba^+}$)
LOWER BAND
FREQUENCY, KHz
10
5
0
1.0
0.5
0
1232:00
:10
:20
:30
:40
:50
1233:00
AMPTE-IRM, DEC. 27, 1984

Figure 7

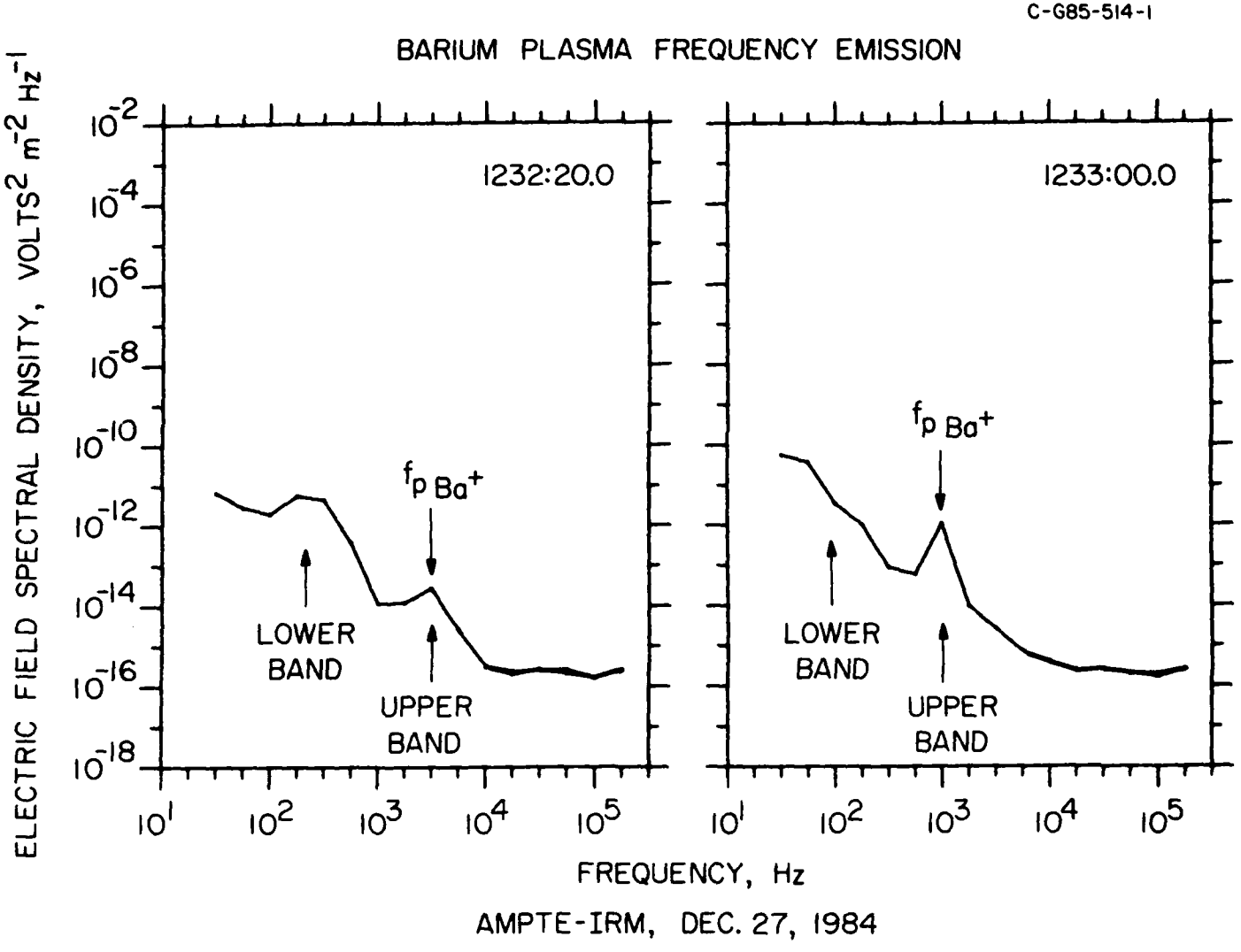
C-G85-514-1
BARIUM PLASMA FREQUENCY EMISSION
ELECTRIC FIELD SPECTRAL DENSITY, VOLTS^2 m^{-2} Hz^{-1}
10^{-2}
10^{-4}
10^{-6}
10^{-8}
10^{-10}
10^{-12}
10^{-14}
10^{-16}
10^{-18}
1232:20.0
1233:00.0
f_p Ba$^+$
LOWER BAND
UPPER BAND
10^1
10^2
10^3
10^4
10^5
FREQUENCY, Hz
AMPTE-IRM, DEC. 27, 1984

Figure 8

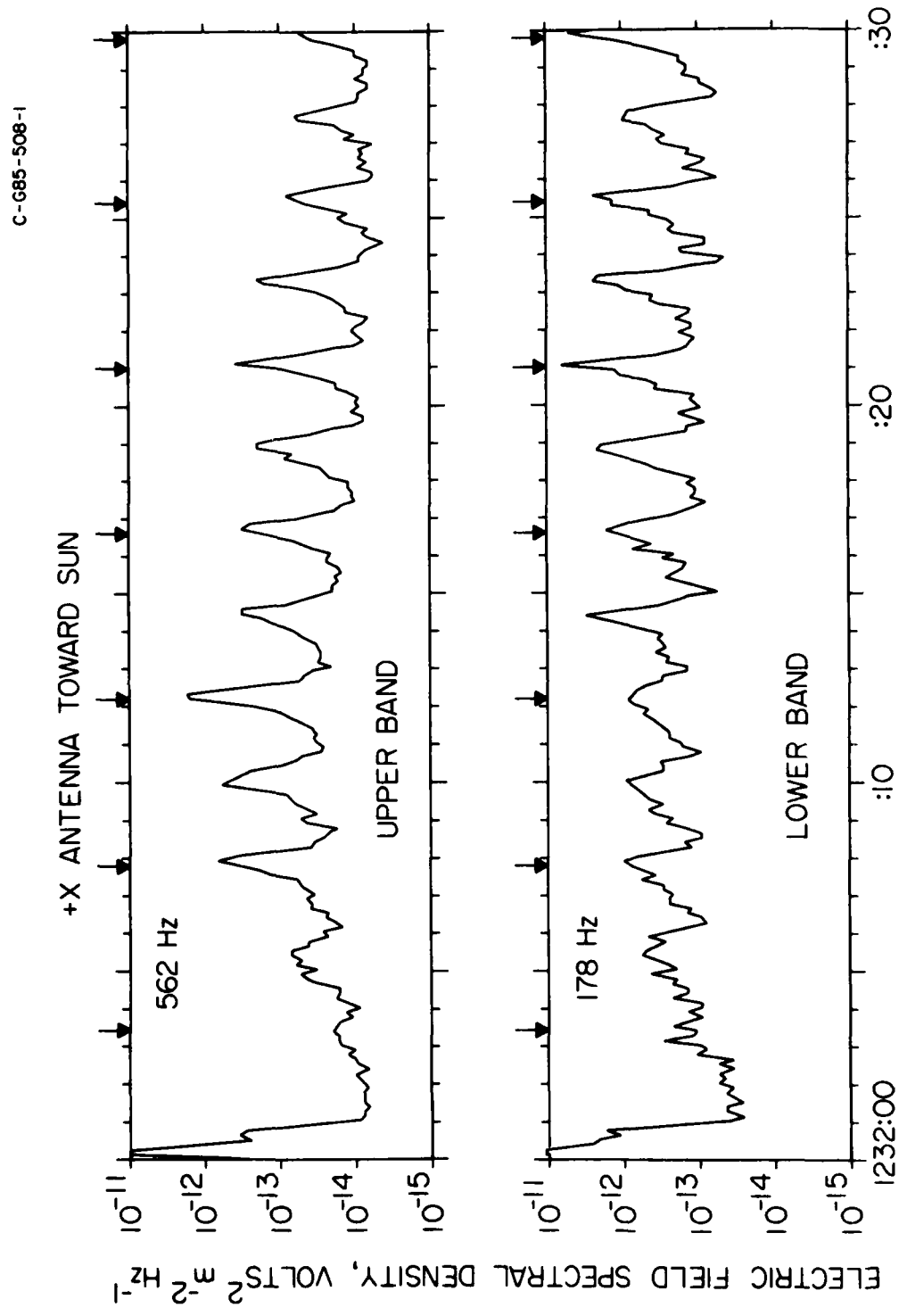
C-G85-508-I
+X ANTENNA TOWARD SUN
562 Hz
UPPER BAND
178 Hz
LOWER BAND
ELECTRIC FIELD SPECTRAL DENSITY, VOLTS² m⁻² Hz⁻¹
10⁻¹¹
10⁻¹²
10⁻¹³
10⁻¹⁴
10⁻¹⁵
1232:00
:10
:20
:30
AMPTE-IRM, DEC. 27, 1984

Figure 9

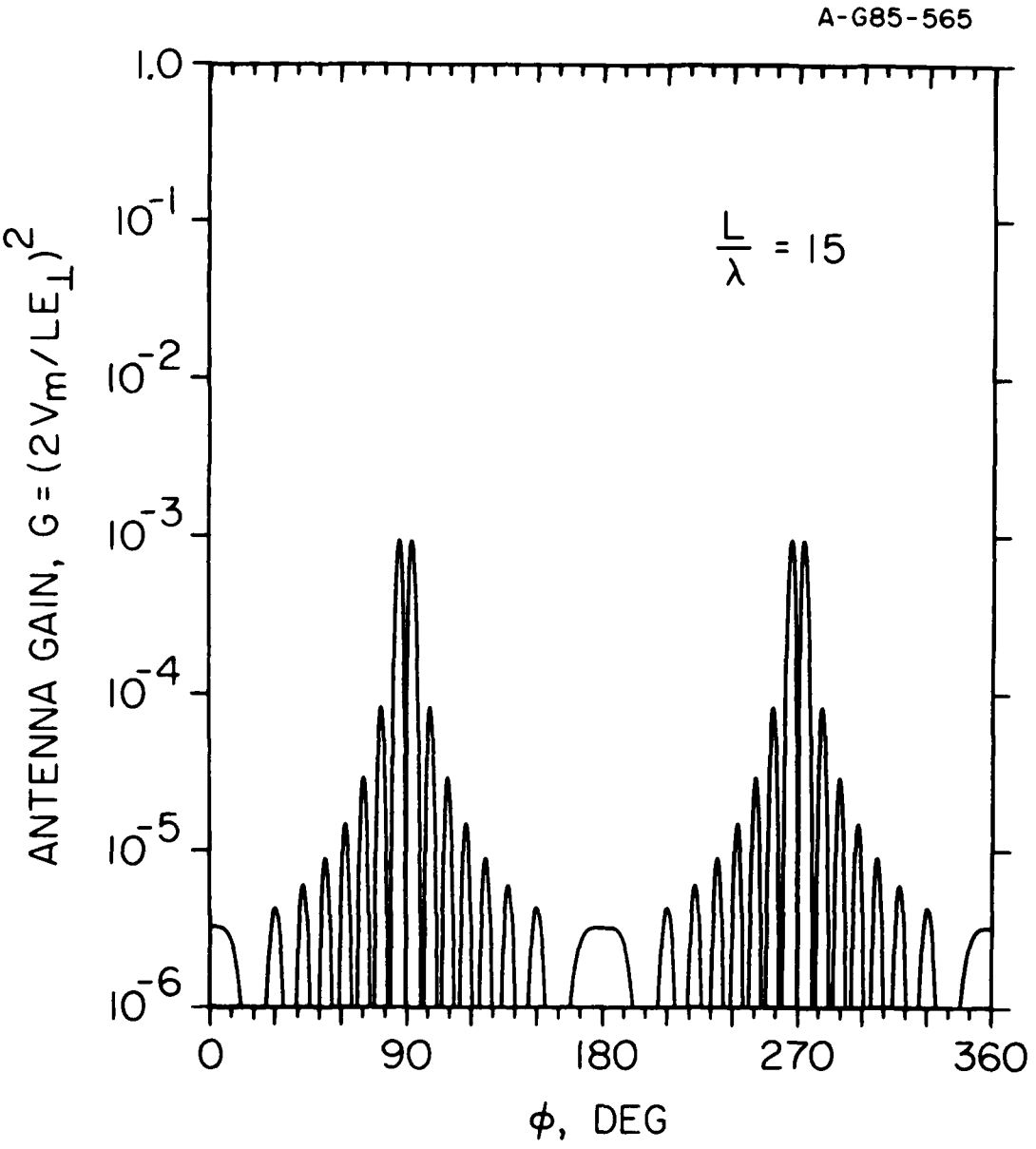
A-G85-565
1.0
10^{-1}
10^{-2}
10^{-3}
10^{-4}
10^{-5}
10^{-6}
$\frac{L}{\lambda} = 15$
ANTENNA GAIN, $G = (2V_m/LE_\perp)^2$
0
90
180
270
360
ϕ, DEG

Figure 10

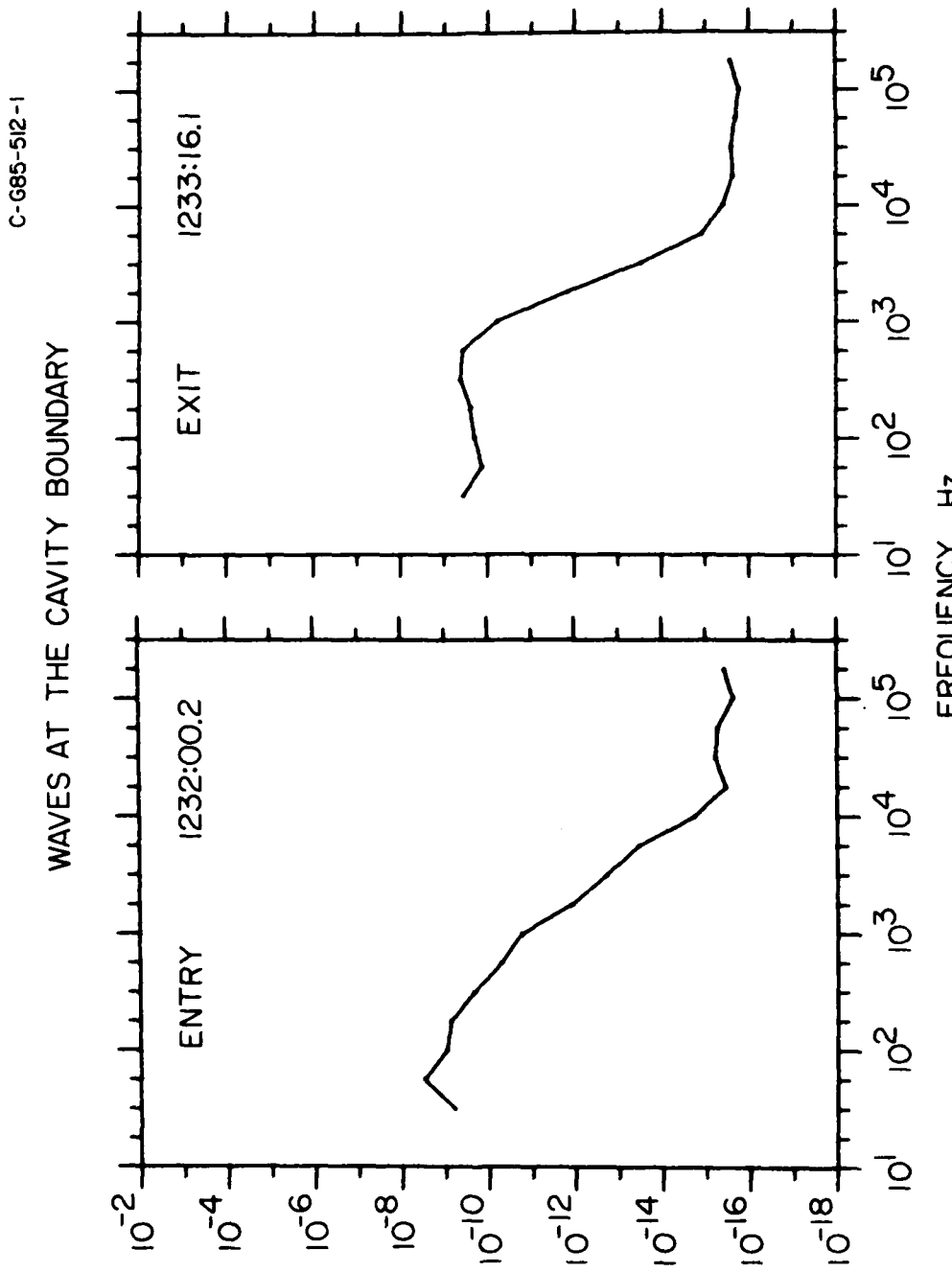
C-685-512-1
WAVES AT THE CAVITY BOUNDARY
ENTRY 1232:00.2
EXIT 1233:16.1
ELECTRIC FIELD SPECTRAL DENSITY, VOLTS² m⁻² Hz⁻¹
FREQUENCY, Hz
AMPTE-IRM, DEC. 27, 1984

Figure 11

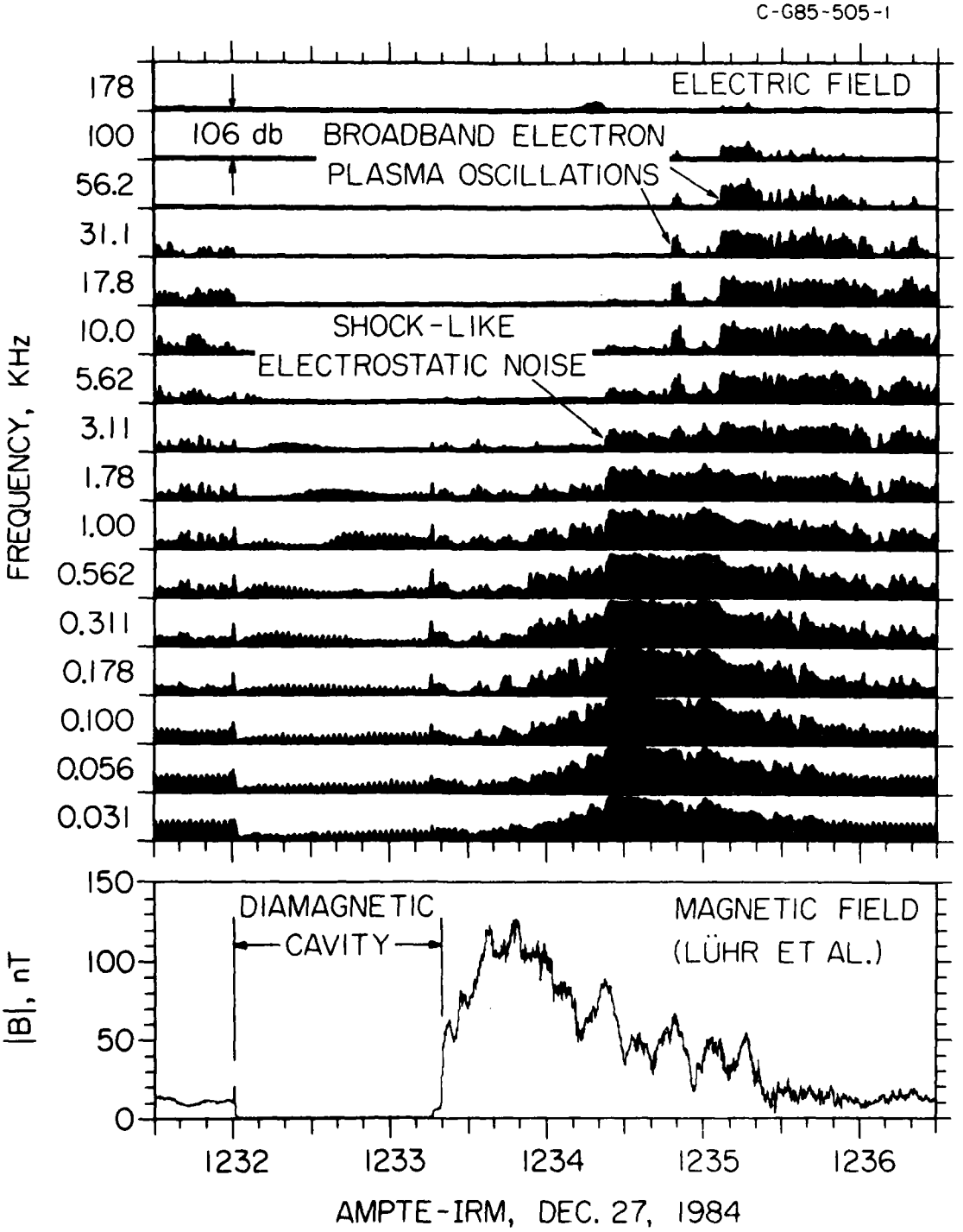
C-G85-505-1
ELECTRIC FIELD
106 db
BROADBAND ELECTRON
PLASMA OSCILLATIONS
SHOCK-LIKE
ELECTROSTATIC NOISE
FREQUENCY, KHz
178
100
56.2
31.1
17.8
10.0
5.62
3.11
1.78
1.00
0.562
0.311
0.178
0.100
0.056
0.031
DIAMAGNETIC
CAVITY
MAGNETIC FIELD
(LÜHR ET AL.)
|B|, nT
150
100
50
0
1232
1233
1234
1235
1236
AMPTE-IRM, DEC. 27, 1984

Figure 12

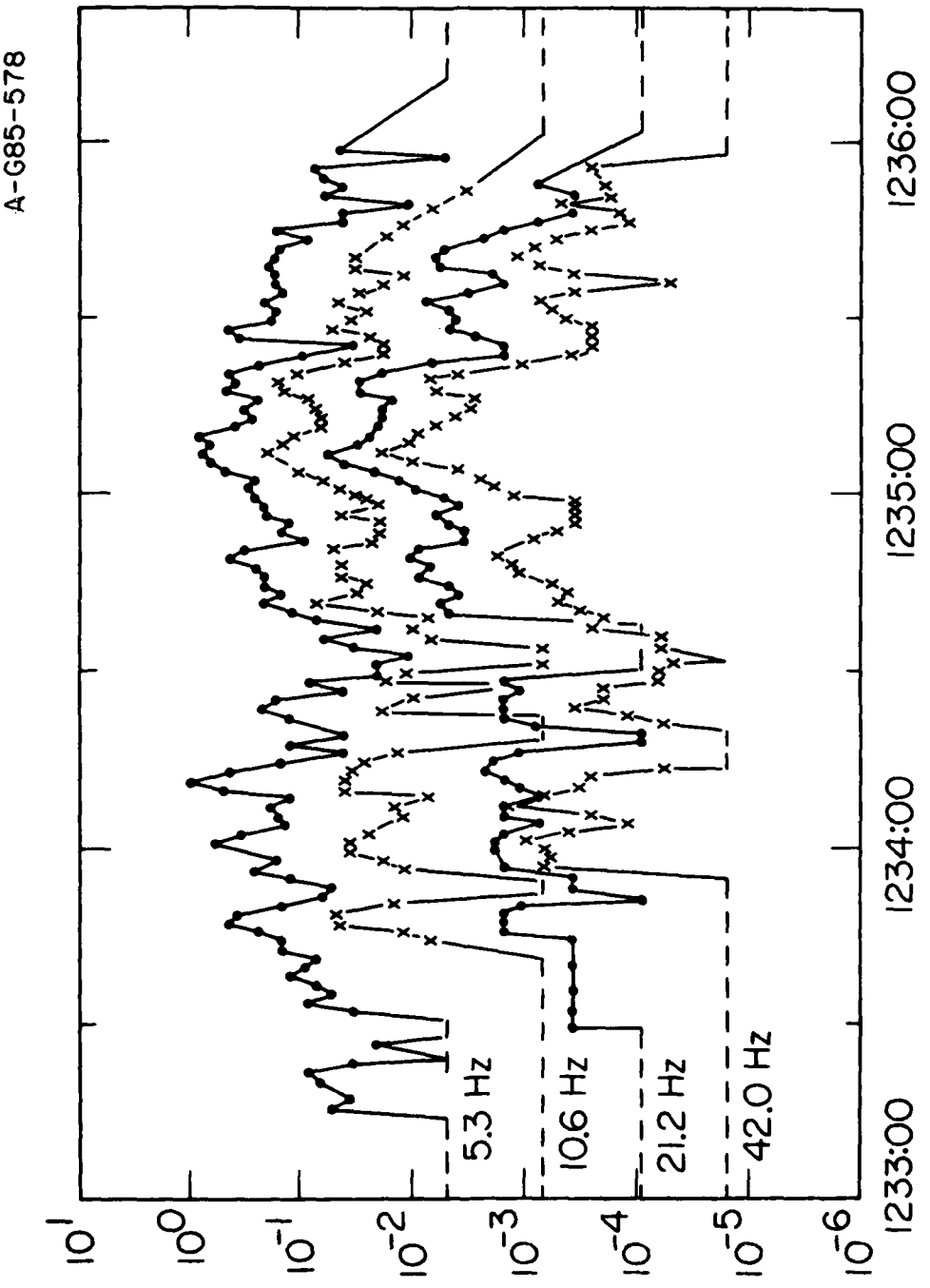
A-G85-578
MAGNETIC FIELD SPECTRAL DENSITY, nT²/Hz
10¹
10⁰
10⁻¹
10⁻²
10⁻³
10⁻⁴
10⁻⁵
10⁻⁶
5.3 Hz
10.6 Hz
21.2 Hz
42.0 Hz
1233:00
1234:00
1235:00
1236:00
AMPTE-IRM, DEC. 27, 1984

Figure 13

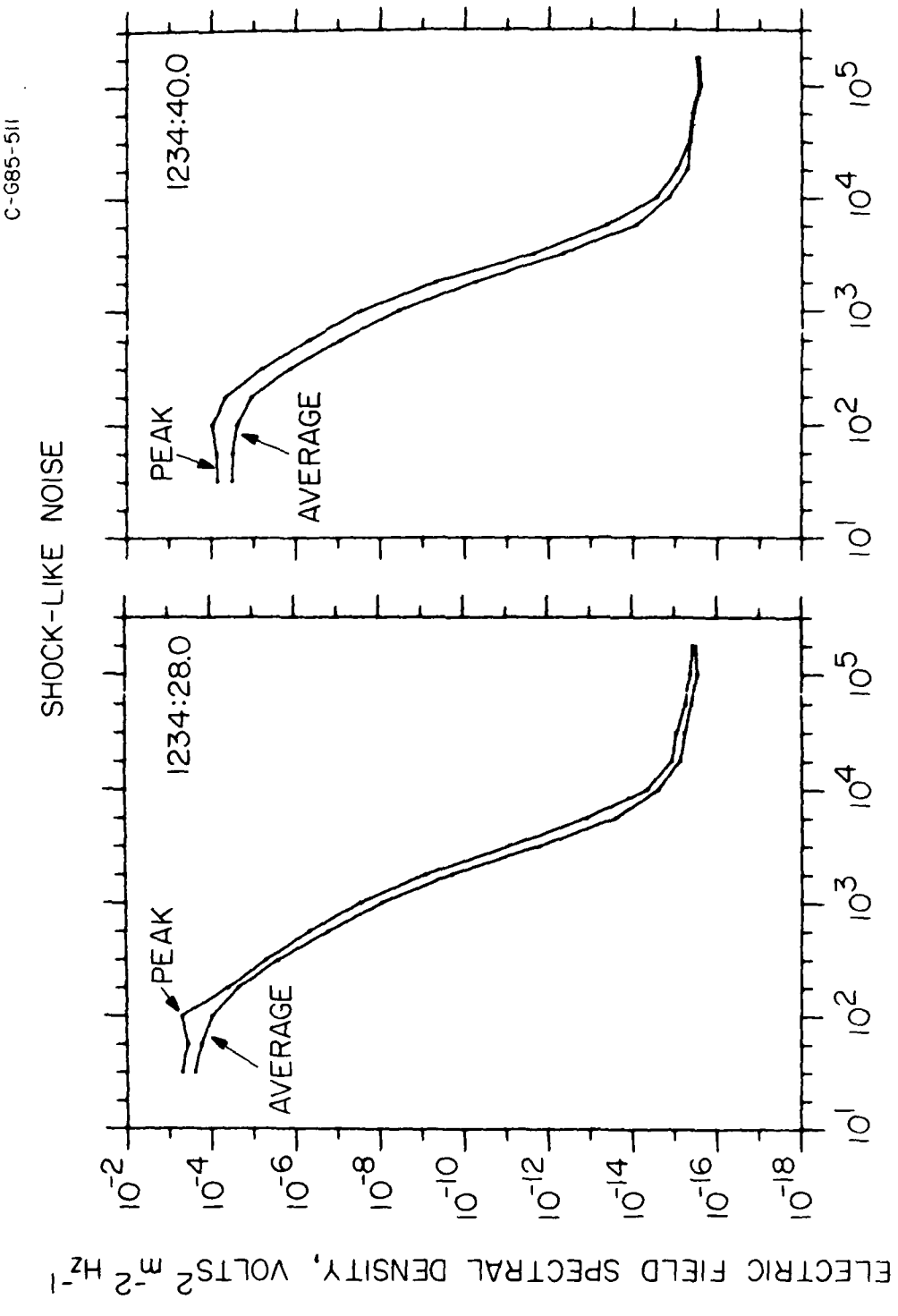
C-G85-511
SHOCK-LIKE NOISE
1234:28.0
1234:40.0
PEAK
AVERAGE
PEAK
AVERAGE
ELECTRIC FIELD SPECTRAL DENSITY, VOLTS² m⁻² Hz⁻¹
FREQUENCY, Hz
AMPTE-IRM, DEC. 27, 1984

Figure 14

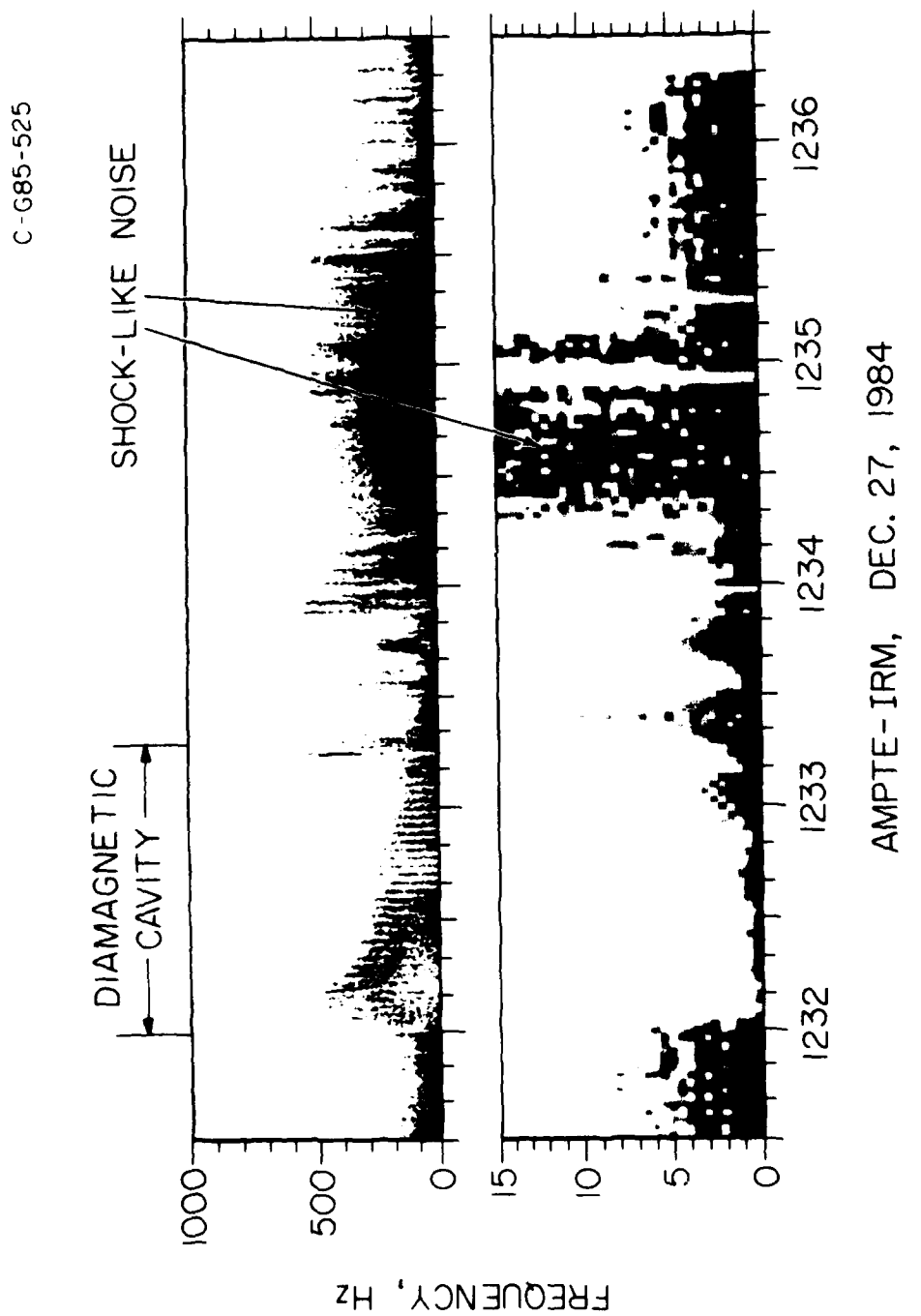
C-G85-525
SHOCK-LIKE NOISE
DIAMAGNETIC CAVITY
1000
500
0
15
10
5
0
FREQUENCY, Hz
1232
1233
1234
1235
1236
AMPTE-IRM, DEC. 27, 1984

Figure 15

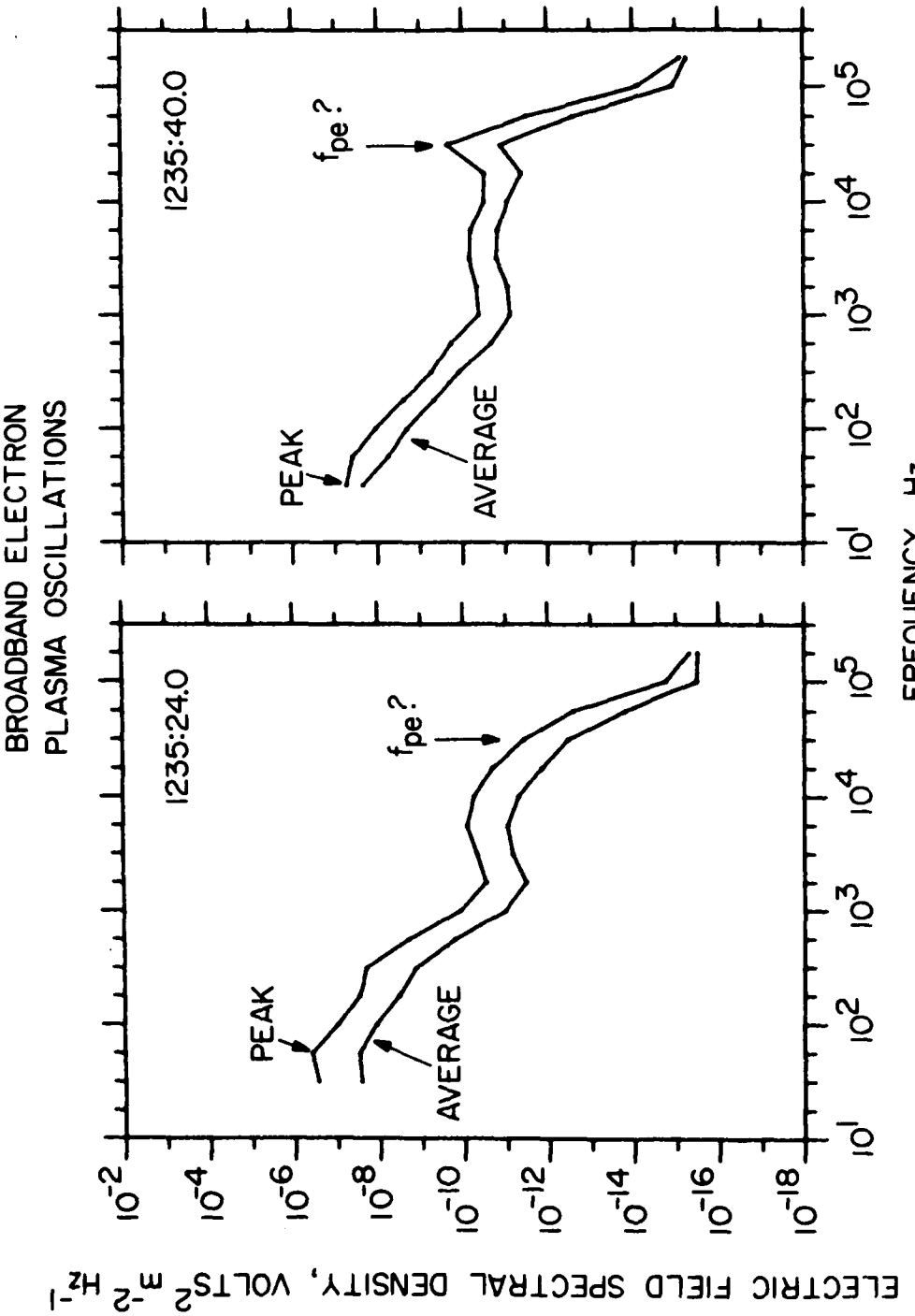
C-G85-513-1
BROADBAND ELECTRON
PLASMA OSCILLATIONS
1235:24.0
1235:40.0
PEAK
AVERAGE
f_{pe}?
ELECTRIC FIELD SPECTRAL DENSITY, VOLTS^2 m^{-2} Hz^{-1}
FREQUENCY, Hz
AMPTE-IRM, DEC. 27, 1984

Figure 16

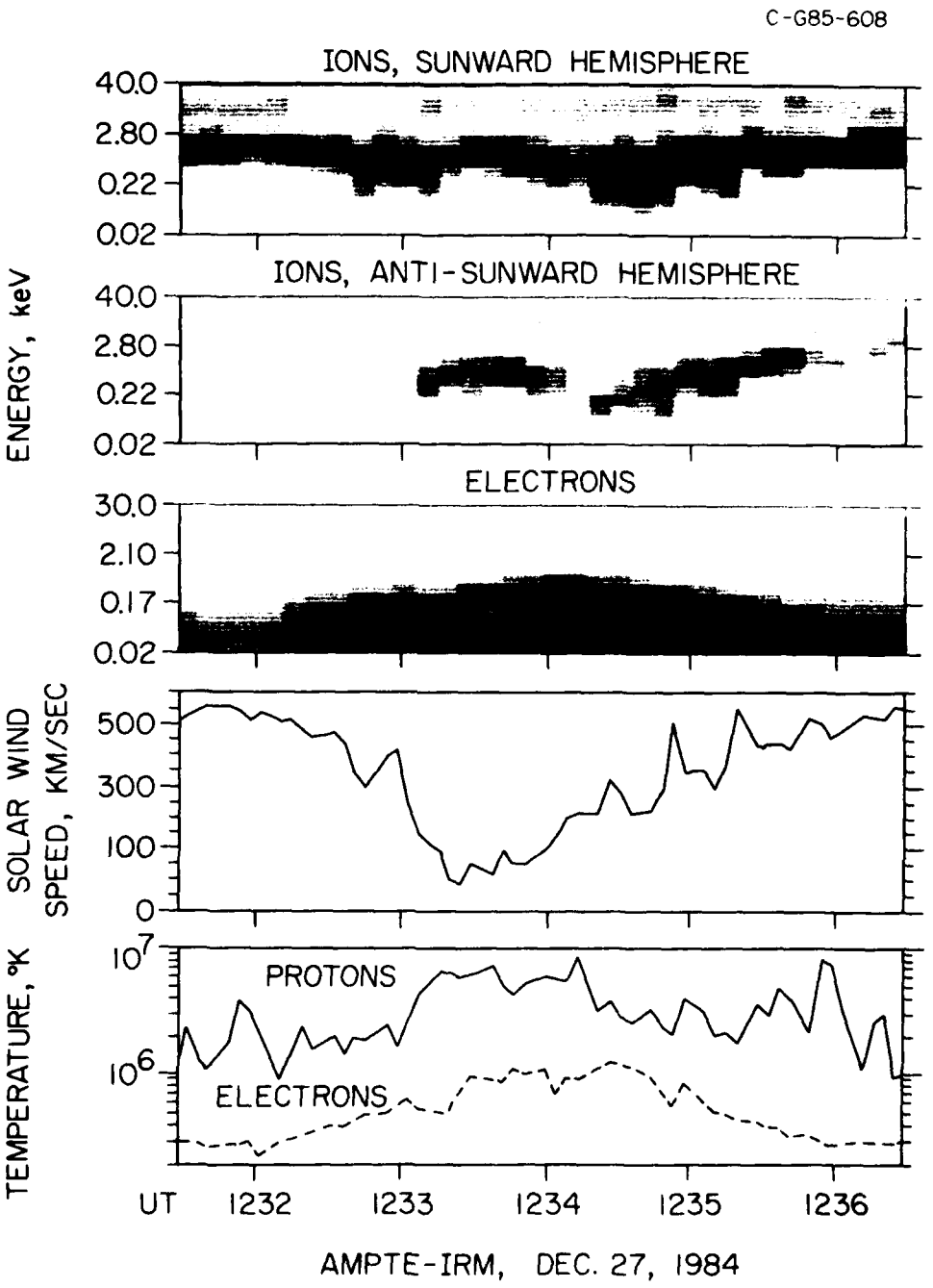
C-G85-608
IONS, SUNWARD HEMISPHERE
40.0
2.80
0.22
0.02
IONS, ANTI-SUNWARD HEMISPHERE
40.0
2.80
0.22
0.02
ENERGY, keV
ELECTRONS
30.0
2.10
0.17
0.02
SOLAR WIND SPEED, KM/SEC
500
300
100
0
TEMPERATURE, °K
10^7
10^6
PROTONS
ELECTRONS
UT
1232
1233
1234
1235
1236
AMPTE-IRM, DEC. 27, 1984

Figure 17

B-G85-65-1

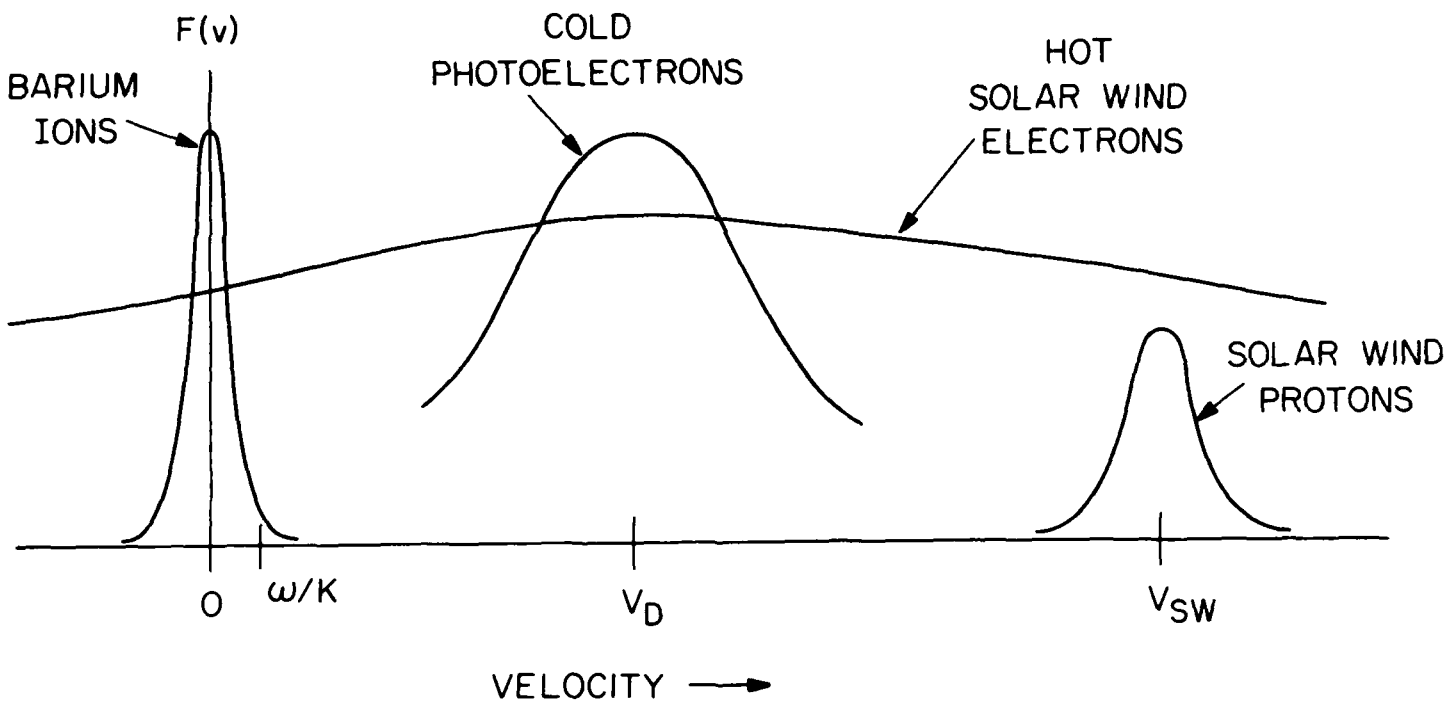

Figure 18

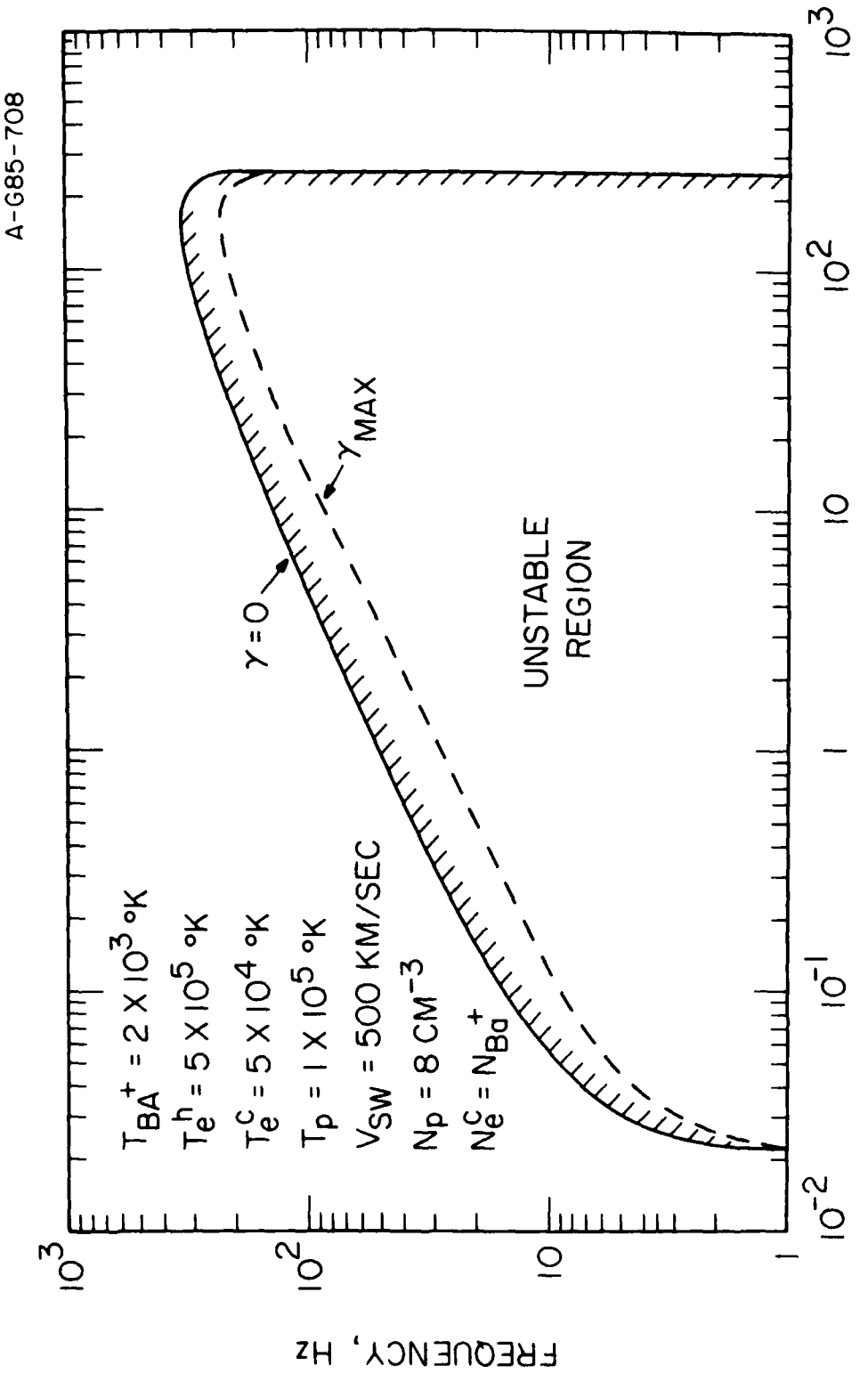
A-685-708
FREQUENCY, Hz
N_{Ba^+}/N_p, BARIUM TO PROTON DENSITY RATIO
10^3
10^2
10
1
10^{-1}
10^{-2}
$T_{BA^+} = 2 \times 10^3$ °K
$T_e^h = 5 \times 10^5$ °K
$T_e^c = 5 \times 10^4$ °K
$T_p = 1 \times 10^5$ °K
$V_{SW} = 500$ KM/SEC
$N_p = 8$ CM^{-3}
$N_e^c = N_{Ba^+}$
$\gamma = 0$
γ_{MAX}
UNSTABLE REGION

Figure 19

A-G85-709

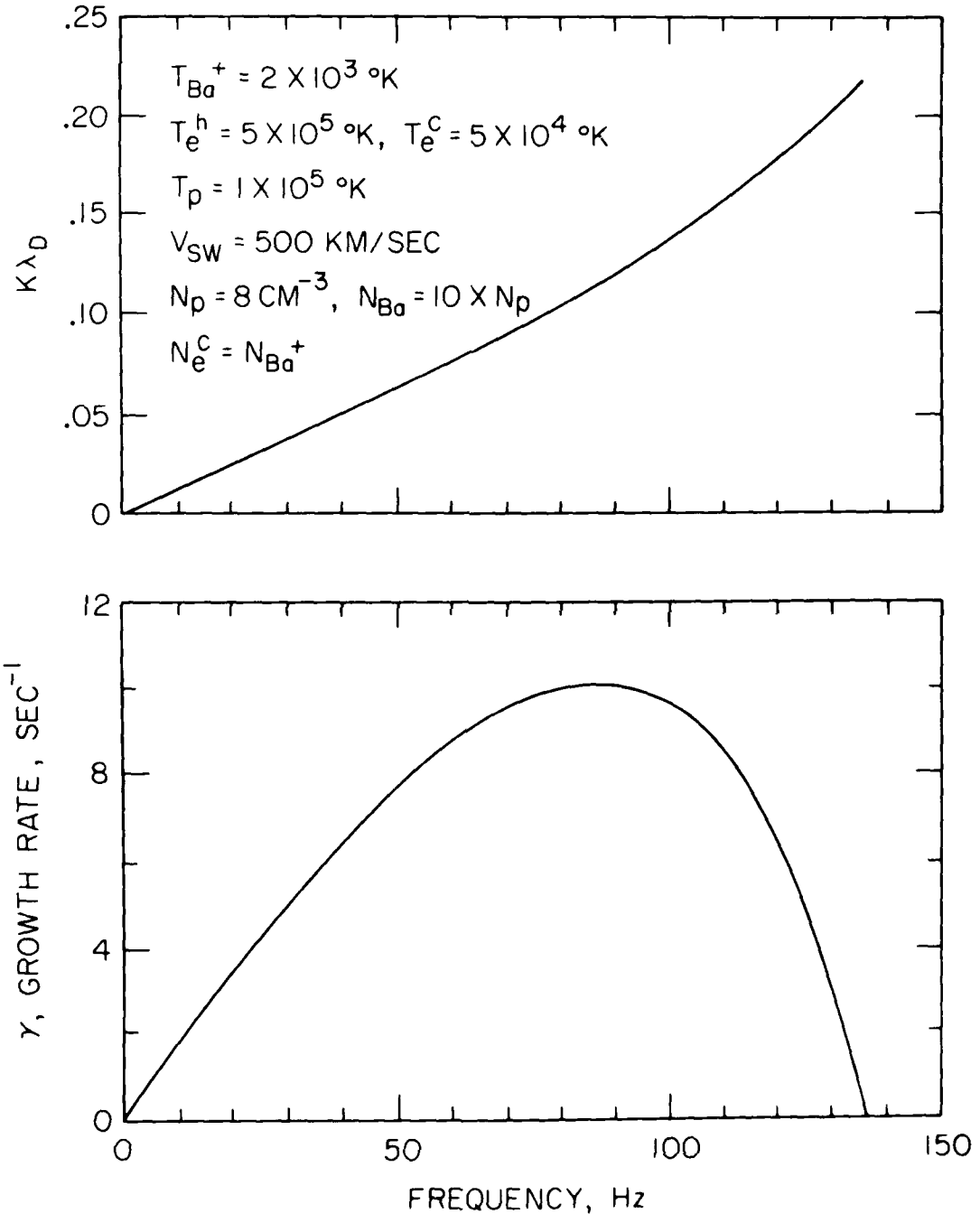

Figure 20

END

FILMED

2-86

DTIC